

1

An Introduction to Nonequilibrium Plasmas at Atmospheric Pressure

Sander Nijdam, Eddie van Veldhuizen, Peter Bruggeman, and Ute Ebert

1.1 Introduction

1.1.1 Nonthermal Plasmas and Electron Energy Distributions

Plasmas are increasingly used for chemical processing of gases such as air, combustion exhaust, or biofuel; for treatment of water and surfaces; as well as for sterilization, plasma deposition, plasma medicine, plasma synthesis and conversion, cleaning, and so on. These plasmas are never in thermal equilibrium – actually, we know of no exemption – and this fact has two main reasons.

- 1) It is easier to apply electromagnetic fields than to uniformly heat and confine a plasma. However, electromagnetic fields naturally transport charged species whose concentrations and energies therefore naturally vary in space, particularly, close to the walls of the container. Generically, the species in such a plasma are not in thermal equilibrium.
- 2) It is energy efficient to not feed energy equally into all degrees of freedom within a gas or plasma, such as into the thermal displacement, rotation, and vibration of neutral molecules, but only into those degrees of freedom that can efficiently create the desired final reaction products for the particular application. Therefore it is frequently preferable to accelerate only electrons to high velocities and let them excite and ionize molecules by impact while keeping the gas cold. If the electron energy distribution is appropriate, some reactions can be triggered very specifically.

In this manner, the nonthermal nature of the plasmas that are created electromagnetically is made into an asset. By varying gas composition, electrode and wall configuration, and circuit characteristics more energy can be channeled into specific excitations and reactions. Recent examples include the optimization of the

pulsed power source for ozone generation in streamer corona reactors [1], or dual frequency RF-generated plasmas [2].

To elaborate the physical understanding further, Mark Kushner has proposed a workshop at the Gaseous Electronics Conference (GEC) 2011 on how the electron energy distribution within a discharge can be tailored for a specific application. A joint approach to this question by theory and experiment now seems within reach because of the large progress of theory in recent years.

1.1.2

Barrier and Corona Streamer Discharges – Discharges at Atmospheric Pressure

The past has mainly seen an experimental approach by trial and error, also guided by some physical understanding. Within the limited space available here, we will review some setups and their physical mode of operation. A common theme is the avoidance of plasma thermalization in the form of arcs and sparks. Variations over two basic approaches are used very commonly and will make the main theme of this review: the corona discharge and the barrier discharge. In a barrier discharge, large currents are suppressed by dielectric barriers on the electrodes. Basically, the discharge evolves only up to the moment when so much charge is deposited on the insulator surfaces that the field over the gas is screened. In a corona discharge, the discharge expands from a needle or wire electrode into outer space where the electric field decreases and finally does not support a discharge anymore. The discharge then has to feed its current into the high-ohmic region of the nonionized gas, which limits the current as well. These two basic principles have seen many variations in the past years and decades. For example, in corona discharges, short and highly ramped voltage pulses create much more efficient streamers that do not cease due to the spatial decrease of the electric field away from the curved electrode but due to the final duration of the voltage pulse.

Both discharge types can (but need not) operate at atmospheric pressure. This poses an advantage as well as a challenge. The advantage lies in the fact that no expensive and complex vacuum systems are required. This makes the design of any reactor a lot simpler, not only when the operating gas is air but also when other gases (such as argon or helium) are used. The challenge consists of the observation that characteristic length scales within the discharge can be much smaller than the discharge vessel and that the discharge can therefore form complex structures, rather than a more or less uniform plasma. These structures have to be understood and used appropriately. For instance, the initial evolution of streamer discharges follows similarity laws [3]: when the gas density is changed, the same voltage will create essentially the same type of streamer, but on different length and timescales. Therefore, streamer fingers and trees grow in a similar manner at 10 μbar as at 1000 mbar, but 10 μbar corresponds to an atmospheric altitude of 83 km where the so-called sprite streamers have a diameter of at least ~ 10 m, while at 1000 mbar, the minimal streamer diameter is $\sim 100 \mu\text{m}$ and conveniently fits into typical experiments.

1.1.3

Other Nonthermal Discharge Types

There is a large variety of nonthermal plasmas. They can be classified into different discharge types, although definitions used by different authors vary significantly. The plasmas or discharges can be classified according to their time dependence (transient or stationary), importance of space charge effects or of heating of the neutral gas species, and presence of a surface close to the discharge. The most important nonthermal plasmas along with their energization method and typical applications are listed in Table 1.1.

This table is intended to give a general idea, but it is far from complete. A further complication is that definitions are used in different ways. For example, in Ref. 8, Braun *et al.* use what they call a microdischarge for ozone generation, whereas the microdischarges as intended in Table 1.1 are much smaller. The microwave discharge made by Hrycak *et al.* [28] qualifies much more for the term *plasmajet* than for microdischarge. More information on the different types of microdischarges is given in [29]; some examples of the use of microdischarges are given in Section 1.4.4.

In many transient discharges, the different discharge types can occur after each other. For example, a discharge can start as an avalanche and then become a streamer, which can develop into a glow and finally into an arc discharge. When applying a DC field between two metal electrodes, a discharge at high pressure will become a thermal arc if the power supply can deliver the current. Nonthermal discharges are, by definition, almost always transient.

Table 1.1 Overview of nonthermal discharge types and their most common applications.

| Type of discharge | Gap (mm) | Plasma | Energization | Typical application | References |
|-------------------------------|----------|-----------|--------------|--|-------------|
| Corona | 10–300 | Filaments | Pulsed/DC | Gas cleaning/dust precipitation | [4, 5] |
| Corona with barrier | 10–30 | Filaments | Pulsed | Gas and water cleaning | [6, 7] |
| Plates/cylinders with barrier | 1–5 | Filaments | AC | Ozone generation/ large surface treatment/ excimer lamps | [8–12] |
| Barrier with packed bed | 3–10 | Filaments | AC | Chemicals conversion | [13–15] |
| Plates with barrier | 1–5 | Diffuse | AC | Surface treatment/deposition | [16, 17] |
| Surface discharge | 1–5 | Filaments | AC | Surface treatment/deposition | [18, 19] |
| Surface barrier | 1–5 | Filaments | Pulsed | Aerodynamic control | [20–22] |
| Plasma jets | 0.5–10 | Diffuse | AC/RF | Local surface | [18, 23–25] |
| Microdischarge | 0.1–1 | Diffuse | AC/RF | Chemicals conversion/ light generation | [26, 27] |

An essential feature of a cold nonthermal discharge is its short duration. Therefore, the largely varying timescales of the processes inside the discharge must be considered. The excitation timescales, which often range from picoseconds to a few microseconds, are clearly not the timescale necessary for preventing thermalization as thermalization occurs in millisecond-order timescales. The critical timescale is basically the characteristic time of the glow-to-spark transition. This transition time can highly depend on conditions such as voltage amplitude and gas composition but is often in the order of a (few) hundred nanoseconds [30]. Dielectric barrier discharges (DBDs) are a well-known example of how (dielectric) barriers can reduce current density and n_e to keep the gas temperature of the discharge low.

Like streamer and avalanche discharges, Townsend and glow discharges are cold discharges. They usually occur as a stationary discharge but have to be preceded by another discharge such as a streamer or avalanche discharge to ignite. In Townsend and glow discharges, electrons are emitted from the electrode and are then multiplied in the gap. In the case of a Townsend discharge, the electron multiplication takes place in the whole gap, while in a glow discharge, space charge concentrates the multiplication in the cathode sheath region. Electrons are freed from the cathode by the temperature of the cathode itself or by secondary emission either due to the impact of energetic positive ions or due to photons or heavy neutrals.

Several cold atmospheric pressure discharges operate in helium. This is not a coincidence as He has a thermal heat conductivity that is about 10 times larger than that of most other gases, which renders heat removal from the discharge to be more efficient. Other methods for efficient heat removal include strongly forced convection cooling in flow stabilized discharges and creation of discharge with a large area-to-volume ratio (microplasmas, see also further) to make the heat losses to the walls more efficient.

1.1.3.1 Transition to Sparks, Arcs, or Leaders

Avalanches, Townsend, streamer, and glow discharges are examples of cold discharges. This means that the heavy particle temperature is not much above room temperature and definitely far below the electron temperature ($T_e \gg T_i \approx T_n$ where e, i, and n stand for electron, ion, and neutral, respectively). At even higher currents, at higher pressures, or with longer pulse durations, these discharges can transform into spark, arc, or leader discharges. These are hot discharges, the heavy particle temperature is close to the electron temperature and can reach thousands of Kelvin ($T_e \gtrsim T_i \approx T_n$). In applications, heating of the gas is often unwanted, and therefore, cold discharges are preferred in many plasma treatment applications.

1.1.4

Microscopic Discharge Mechanisms

1.1.4.1 Bulk Ionization Mechanisms

The main ionization mechanism in electric discharges is impact ionization; in attaching gases such as air, impact ionization is counteracted by electron attachment.

Other mechanisms that create free electrons such as photoionization or electron detachment from negative ions are discussed in Section 1.2.4.1. Impact ionization occurs when electrons are accelerated in a high local electric field. At a certain kinetic energy, they can ionize background gas atoms or molecules and create more electrons. In air, this occurs by the following reactions:



In the so-called local field approximation (i.e., when the reaction rate is approximated as depending on the local electron density and local electric field only) [31, 32], the number of electrons generated per unit length per electron is called the *Townsend impact ionization coefficient* $\alpha_i(|E|) = \sigma_i(|E|) \cdot n_0$. Here \mathbf{E} is the electric field, σ_i the cross section for electron impact ionization, and n_0 is the background gas density. An old and much used approximation is

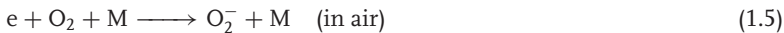
$$\alpha_i(|E|) = \alpha_0 \exp(-E_0/|E|) \quad (1.3)$$

This notation illustrates that the Townsend coefficient is characterized by two parameters: E_0 characterizes the electric field where impact ionization is important; this electric field is proportional to the gas density n_0 . α_0 characterizes the inverse of the ionization length at these fields. More precisely, $1/\alpha_i(|E|)$ is the mean length that an electron drifts in the field \mathbf{E} before it creates an electron–ion pair by impact. Therefore, in geometries smaller than this length, no gas discharge can occur. Both the electron mean free path, between any collision, and the ionization length scale with inverse gas density.

The electron loss rate due to electron attachment on attaching gas components has a similar functional dependence as the impact ionization rate, but different parameters. One needs to distinguish between dissociative attachment



and three-body attachment



where M is an arbitrary third-body collider, for example, N_2 or O_2 . As a third body is required here to conserve energy and momentum, the importance of three-body attachment relative to dissociative attachment increases with density. Dissociative attachment scales with gas density in the same manner as the impact ionization reaction, while three-body attachment is favored at higher gas density. On the other hand, dissociative attachment becomes more important at higher electric fields, even at standard temperature and pressure. For detailed discussions of the derivation of these reaction coefficients, we refer to [33–36].

The *breakdown field* is defined as the field where impact ionization and electron attachment precisely balance; at higher electric fields, an ionization reaction sets in. The spatial and temporal evolution of the discharge depends on the distribution of electrons and electric fields; this is discussed in more detail below.

1.1.4.2 Surface Ionization Mechanisms

Next to the bulk gas, the presence of a dielectric or metallic surface can also affect the discharge significantly. It will modify the electric field configuration, and it is able to provide electrons. Dielectrics can also store surface charges [37] and prevent charge carrier flow through the surface.

Electrons can be freed from a surface by high fields or by secondary emission on impact of ions [38], fast neutrals, or (UV) photons [39]. Photons can be generated in the bulk of the discharge and then free an electron from the surface. Electron emission can be enhanced by the local electric field at the surface or by higher surface temperatures. The freed electrons can form the start of an avalanche, which enables the discharge to initiate or propagate (over the surface). See Section 1.4.3 for a more elaborate discussion on this topic.

1.1.5

Chemical Activity

The main advantage of nonthermal plasmas is their high chemical efficiency. As little or no heat is produced, nearly all input energy is converted to energetic electrons. This is in contrast to thermal plasmas in which the heating itself leads to higher thermal losses and thereby can be a waste of energy, which reduces the chemical efficiency of these hot plasmas [40] and can damage walls and other nearby surfaces (such as the substrate in a surface processing application). Furthermore, higher gas temperatures will change the reaction kinetics which, amongst others, may lead to breakdown of ozone and increased formation of NO_x . Of course, the different reaction kinetics of higher gas temperatures can also be beneficial for some chemical reactions such as destruction of hydrocarbons.

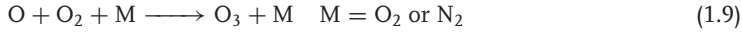
The fast electrons produced in a nonthermal plasma can have energies of the order 10 eV or even higher and can therefore trigger many different chemical processes. Besides fast electrons, energetic photons can also play a role in the reactions in a nonthermal plasma. One important example of such a reaction is photoionization in air, which is discussed in detail in Section 1.2.4.1. However, the primary source of all reactions is electron impact on the bulk gas molecules, which leads to many reactive species that can then further react with more stable species. Examples of the reactive species are OH, O, and N radicals; excited N_2 molecules; and atomic and molecular ions (e.g., O^+ , O_2^+).

One of the main paths of chemical activity in nonthermal plasmas in air is ozone production. This is generally believed to be a two-step process as described by Chang *et al.* [41] and Ono and Oda [42].

- 1) First, free oxygen radicals are produced by inelastic electron impact.



2) Then, ozone is created by reactions of these free radicals.



Ozone can be produced with a wide range of electrode and discharge topologies, many of which are treated below; the most popular are dielectric barrier discharges. An early example is the ozone generator of Siemens made in 1857. The most important application of this device was ozone production for disinfection of water. Even now, this device is used, with only minor modifications [43]. But corona discharges can create O radicals (and thereby ozone) with very high energy efficiency as well [1], as will be discussed in more detail further below. In commercial ionizers, pure oxygen is often used as the starting gas because the nitrogen that is present in air can lead to the formation of NO_x (a general term used for NO and NO_2 and sometimes other nitrogen–oxygen compounds) with the following reactions [44]:



where the O radicals come from Eqs. (1.6–1.8) and the N radicals are produced by [45]



The produced NO can further react with NO_2 as described in [45, 46]



However, nonthermal plasmas can also remove NO from gas streams. The main path for the removal of NO from air at low NO concentrations is (Eq. (1.12)) followed by [47]



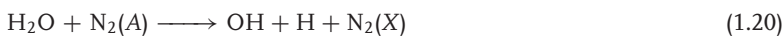
A second type of radical that is important in nonthermal plasmas is OH. This is produced in moist gases (e.g., moist air) by the following reaction [48]:



Note that apart from electron-induced dissociation, dissociative electron recombination of water containing ions can also efficiently produce OH.



The rate of this reaction for nonthermal discharges with T_e in the range 1–2 eV is sometimes even faster than electron dissociation [49]. Several secondary reactions are also believed to play an important role in the production of OH



where $O(^1D)$ is an excited state of atomic oxygen, $N_2(A)$ is a metastable nitrogen molecule and $N_2(X)$ is a nitrogen molecule in the ground state. It is clear that Eq. (1.17) occurs only in the ionizing phase, while Eqs. (1.18–1.20) also occur in the recombining phase when the electron temperature is equal to the gas temperature.

Which reactions dominate depends on the electron energy (which is dependent on topology, voltage shape, and amplitude, etc.) and the composition of the gas. In general, thermal discharges mostly produce NO_x , while nonthermal discharges produce ozone instead and can remove NO_x when concentrations are high. At low NO_x concentrations also, nonthermal discharges can lead to the net production of NO_x . A comparison of NO_x production by sparks and corona discharges was performed by Rehbein and Cooray [50]. They found that sparks produce about 2 orders of magnitude more NO_x per Joule than corona discharges. Overviews of different reactive species and the conditions in which they are important are given by Eliasson and Kogelschatz [51] and Kim [43].

Besides NO_x removal, which was discussed above, a host of other species can be removed from gas streams by nonthermal plasmas. Examples are volatile organic compounds (VOCs), chlorofluorocarbons (CFCs), SO_2 , odors, and living cells (in disinfection or sterilization).

Most charges in a nonthermal discharge in air are initially produced by the direct impact ionization of nitrogen



with a threshold ionization energy of 15.58 eV or of oxygen (Eq. (1.1)) with a threshold ionization energy of 12.07 eV. According to Aleksandrov and Bazelyan [52], N_2^+ and O_2^+ will quickly change to other species according to the following scheme (for dry air under standard conditions):



After some tens of nanoseconds, the positive ions are dominated by O_4^+ . Electrons are quickly attached to molecular oxygen by reactions given in Eqs. (1.4) and (1.5).

1.1.6

Diagnostics

In all nonthermal plasmas, fast electrons excite species. Many of the excited species can fall back to lower excited levels or the ground level and thereby emit a photon. These photon emissions are by far the most important property of cold discharges that are studied experimentally. They are used for imaging and for optical emission spectroscopy. Spectra of cold discharges in air are dominated by the emissions of the second positive systems of N_2 (SPSs, upper states $B^3\Pi_g$ and $C^3\Pi_u$). The SPS is often used to obtain the rotational temperature, which is mostly a good indication of the gas temperature [53].

For strongly pulsed and high field discharges and also in discharges in, for example, He with air impurities, the first negative system of N_2^+ (FNS, upper state $B^2\Sigma_u^+$) readily occurs. Relative intensity comparisons of the SPS and this FNS have

been performed by many authors and are used to determine the electric field in nitrogen-containing discharges. This method is employed, for example, by Kozlov *et al.* [54] for laboratory scale discharges and by Liu *et al.* [55] for sprites.

There are many other rotational bands of different molecules that can be used to obtain rotational temperatures, which are mostly a good indication of the gas temperature. Especially popular is the UV emission band of OH(A–X) around 309 nm [53]. However, it has recently been found that the rotational population distribution is not always in equilibrium with the gas temperature and sometimes leads to overestimates [56].

Electron densities above 10^{20} m^{-3} can be determined by measuring the Stark broadening of the hydrogen Balmer lines. Especially the Balmer β line is very popular. It is important to note that it is necessary to carefully take into account all broadening mechanisms including van der Waals broadening, which can become quite important for low-temperature atmospheric pressure plasmas. A detailed description can be found in [53].

Besides (passive) optical emission spectroscopy, there are many other techniques to study nonthermal plasmas. Apart from standard voltage and current waveform measurements, several electrical probes exist, especially developed for low pressure plasmas, although it is often difficult and very complicated to apply them on atmospheric pressure plasmas. The active laser spectroscopy techniques have developed into a wide field. The techniques most commonly applied to atmospheric pressure plasmas include laser-induced fluorescence (LIF) and two-photon-absorption laser-induced fluorescence (TALIF), which are good ways to obtain information on the chemical composition of radicals. With proper calibration, even absolute densities can be obtained [57, 58]. Other well-known laser-based techniques are based on scattering of photons. Thomson scattering can give direct information on the electron density and temperature [59, 60]. Rayleigh and Raman scattering provide information on gas density and temperatures. The conceptually simplest active technique is absorption spectroscopy (often also performed with lasers). This technique is used to determine absolute densities of certain species, often in the ground state (e.g., OH). Radical density fluxes can also be obtained by appearance potential mass spectrometry [61]. Mass spectrometry also gives the possibility to measure the ion flux of one of the electrodes directly and determine the ion composition of the plasma [62].

1.2

Coronas and Streamers

1.2.1

Occurrence and Applications

Streamers are the earliest stage of electric breakdown of large nonionized regions. They precede sparks and create the path for lightning leaders; they also occur as

enormous sprite discharges, far above thunderclouds. Streamers and the subsequent electric breakdown are a threat to most high-voltage technology.

However, streamers are also used in a variety of applications and are appreciated for their energy-efficient plasma processing. The following is an (incomplete) application list:

- Gas and water cleaning: The chemical active species that are produced by streamers can break up unwanted molecules in industrially polluted gas and water streams. Contaminants that can be removed include organic compounds (including odors), NO_x , SO_2 , and tar [3, 6, 63, 64].
- Ozone generation: By simply applying a streamer discharge in air, first O^* radicals and then ozone is created. The low temperature in a streamer discharge limits the destruction of the produced ozone. The ozone can be used for different purposes such as disinfection of medical equipment, sanitizing of swimming pools, manufacturing of chemical compounds, and more [4].
- Particle charging: A negative DC corona discharge can charge dust particles in a gas flow. These charged dust particles can now be extracted from the gas by electrostatic attraction. Such a system is called an electrostatic precipitator (ESP) and is used in the utility, iron/steel, paper manufacturing, and cement and ore-processing industries. Similar charging methods are used in copying machines and laser printers [4, 65].

A corona discharge is (an often DC-driven) discharge in which many streamers are initiated from one electrode and, depending on the conditions, may or may not reach another electrode. The name corona comes from the crownlike appearance of the many streamer channels around the primary (driven) electrode.

Traditionally, DC corona discharges are classified in several different forms depending on the field polarity and electrode configuration [41]. In case of a positive point-plane discharge, one can recognize the burst pulse corona, streamer corona, glow corona, and spark for an increase in applied voltage. In a negative point-plane corona, this is replaced by a Trichel pulse corona, a pulseless corona, and again, a spark.

Since the 1980s, corona discharges are separated into two different categories: continuous and pulsed. Continuous corona discharges occur at DC or low-frequency AC voltages. If the circuit providing the voltage can support high currents, these will transform into a stationary glow or spark discharge. Therefore, continuous corona discharges can only occur if the current is limited. One example is a continuous corona discharge around high-voltage power lines, where the large gap to the ground limits the current. A recent example of work on DC-excited corona discharges is by Eichwald *et al.* [66].

The current of a continuously excited corona is often spiked because the discharge is not really continuous but is self-repetitive in nature. In such a self-repetitive corona, the discharge stops itself due to the buildup of space charge near the electrode tip. Only after this space charge has disappeared by diffusion and drift will a new discharge occur [67].

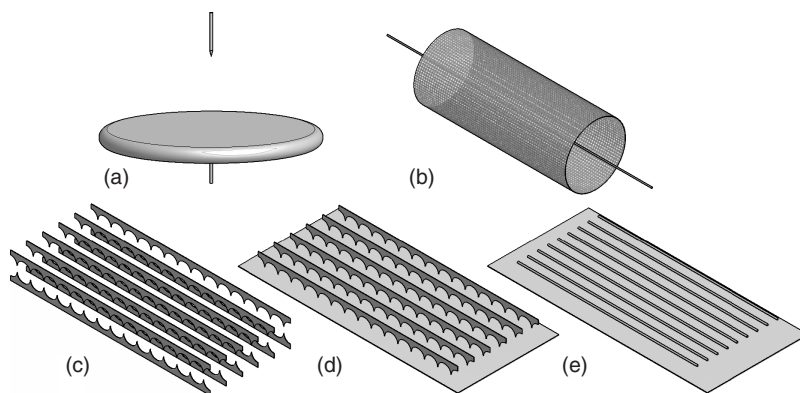


Figure 1.1 Schematic depictions of popular electrode geometries in corona reactors: (a) point-plane, (b) wire-cylinder, (c) double sawblade, (d) sawblade-plane, and (e) wire-plane. The high voltage is applied to the following parts: (a) top needle, (b) central wire, and (c–e) top sawblade/wires. The other parts are grounded.

A pulsed corona is produced by applying a short (usually submicrosecond) voltage pulse to an electrode. Its practical advantages are that the short duration of the pulse ensures that no transition to spark takes place, therefore it can be used at voltages and currents higher than that at continuous corona can be used.

Shang and Wu [68] have shown that a positive-polarity-pulsed corona removes more NO than a negative polarity discharge. van Heesch *et al.* [1] show that negative coronas have a higher efficiency in the production of O^* radicals (about a factor of 2 higher).

In laboratory studies of corona discharges, the most popular geometry is a point-plane geometry (Figure 1.1a), where a needle is placed above a grounded plane. The high voltage (pulse) is applied to the needle electrode. However, for industrial applications, this geometry is not sufficient, as it does not fill the whole gas volume with the discharge. The most popular geometries in industrial applications are the wire-cylinder, wire-plate, and the saw-blade geometries [41, 69]. See Figure 1.1b–e for schematic images of these geometries.

The wire-cylinder geometry is probably used the most. It ensures a quite homogeneous distribution of the discharge and is easy to implement in a gas-flow system. Often, multiple wire-cylinder reactors are mounted in parallel with regard to the gas flow to enable high gas throughput.

1.2.2

Main Properties of Streamers

Streamers are rapidly extending ionized fingers that can appear in gases, liquids, and solids. They are generated by high electric fields but can penetrate into areas where the background electric field is below the ionization threshold due to the

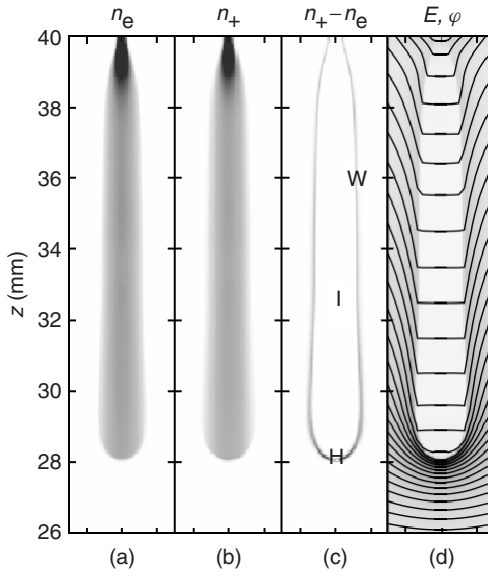


Figure 1.2 Structure of positive streamers shown by zooming into the relevant region of a simulation by Ratushnaya *et al.* The panels show (a) electron density n_e , (b) ion density n_+ , (c) space charge density ($n_+ - n_e$), as well as (d) electric field strength E and equipotential lines φ . The letters in (c) indicate the streamer regions: H – streamer head, I – interior, and W – wall of the streamer channel. (Source: Image from Ref. [71].)

strong field enhancement at their tip. The mechanism of field enhancement is illustrated in Figure 1.2, which shows the simulation of a positive streamer in air at standard temperature and pressure; for details we refer the readers to [70, 71]. The plots show electron and ion density, space charge, and field distribution. The plots can be understood as follows. Panels (a) and (b) show that the interior of the streamer channel consists of a conducting plasma with roughly the same electron and ion densities. The electric field (panel d) in this ionized area is largely screened by the thin space charge layer shown in panel (c).¹⁾ In front of the ionized finger, the space charge layer is strongly curved, and therefore, it significantly enhances the electric field in the nonionized area ahead of it. This self-organization mechanism due to space charge effects makes the streamer a well-defined nonlinear structure; gas heating is negligible in most cases.

As described in a previous streamer review for geophysicists [3], the electrons in the high-field zone at the streamer head are very far from equilibrium. The electron energy distribution can develop a long tail at high energies, and it is now known that electrons at the tip of negative streamers can even run away

1) We remark that in the older literature and in many books the space charge is smeared out over the complete streamer head and only simulations in the past 25 years have

shown that it is concentrated in a thin layer. This is important for the streamer electrodynamics.

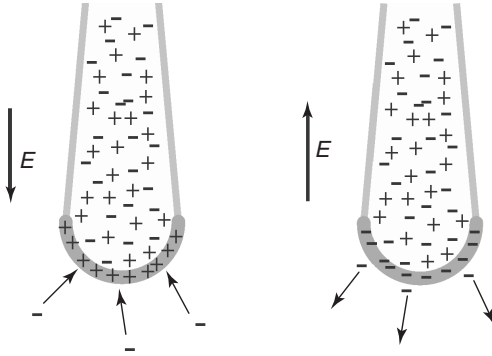


Figure 1.3 Illustration of downward propagating positive (a) and negative (b) streamers. The plus symbols indicate positive ions, while the minus symbols indicate negative ions or free electrons.

[31, 72–75], if the field enhancement is above 180 kV cm^{-1} in STP air, corresponding to 720 Td. This is the current explanation for the hard X-rays emitted during the early streamer-leader phase of MV-driven pulses [76]. How to optimize the electron energy distribution for a particular plasma processing purpose is a current research question.

The fact that streamer velocities and diameters can vary substantially between different electrode geometries and electric circuits is by now well established [5, 77, 78]. Simulations show that the maximum of the enhanced electric field also varies substantially, as reviewed recently in [79].

The maximal field determines the ionization rate inside the streamer [31, 70, 80] and, therefore, the excitation rates for gas processing purposes. The search for optimal processing conditions determined by both the electron energy distribution and the ionization rate is currently underway, both theoretically and through the development of optimized electric circuits. Here it should be mentioned that very short voltage rise times create much thicker [5, 77, 78] and more efficient streamers [1].

An important distinction is between positive and negative streamers, where the polarity refers to the net charge at their tips (Figure 1.3). They are also known as *cathode- or anode-directed streamers*. A negative streamer moves in the electron drift direction, and as the streamer velocity is frequently comparable to the local electron drift velocity,²⁾ its motion can be explained by purely local mechanisms. On the contrary, a positive streamer moves, in most cases, even faster [78]. The reason for this counterintuitive behavior lies in the fact that the relative immobility of the ions in the space charge layer around the positive streamer keeps the streamer finger thin and focused; therefore the electric field at the tip can be much higher [81]. The mechanism allowing positive streamers to propagate is explained below.

2) The older Russian literature frequently states that the streamer velocity would be much larger than the electron drift velocity,

but there the local field enhancement and local drift velocities are not characterized very carefully.

Concerning theory and simulations, there are currently three models: (i) Monte Carlo and (ii) hybrid models that follow the single-electron dynamics within a streamer, but are still constrained to rather short streamers, fluid, or density models, which now also start to treat the interaction of streamers, but cannot resolve the electron energy distribution, and (iii) moving boundary models where the thin space charge layer around the streamer is treated as a moving boundary. Currently, reviews of all three model classes have been published or are under review; we refer the reader for details to [71, 82, 83].

1.2.3

Streamer Initiation or Homogeneous Breakdown

When a discharge starts to develop, there are only few free charge carriers present, and therefore the electric field is not modified by space charge effects yet. The discharge is then said to be in the avalanche phase where free charge carriers multiply in regions where the electric field is above the breakdown value.

The discharge can then evolve either in a more homogeneous or a more streamerlike manner. If the initial ionization seed is very localized (e.g., because it evolves out of a single electron or because a macroscopic seed is ejected from a pointed needle electrode), or if the electric field is above breakdown only in a small part of space (again, e.g., close to a needle electrode), a localized structure such as a streamer that carries a field enhancement forward at its tip can emerge. On the other hand, if there is a higher level of preionization and if the electric field is at most places above the breakdown value, a more homogeneous discharge will emerge [84].

If a single electron or a very localized seed is placed in a homogeneous field above the breakdown value, Raether and Meek estimated in the late 1930s, that space charge effects set in and a streamer initiates when the total number of free electrons reaches 10^8 – 10^9 in air at standard temperature and pressure [85, 86]. However, this estimate is independent of the electric field. Taking into account that an electron avalanche grows with a slower rate in a weaker field, but that their diffusive broadening is essentially the same, a correction to the so-called Raether–Meek criterion was developed by Montijn and Ebert [87].

However, in most streamer experiments and applications, streamers are generated from a tip- or wirelike structure and not in a homogeneous field. At such a (sharp) tip or wire, the electric field will be greatly enhanced, which makes it easier to initiate a streamer. After initiation, the streamer can propagate into the rest of the gap where the background field may be too low for streamer initiation, but high enough for streamer propagation (discussed in the next section). Such a geometry with field enhancement greatly reduces the required voltages for streamer initiation, which makes experiments and applications smaller, cheaper, and easier to operate.

The lowest voltage at which a streamer can initiate from a pointed electrode is called the *inception voltage*; it depends on electrode shape and material as well as on gas composition and density and (up to now) has no direct interpretation in terms of microscopic discharge properties yet.

1.2.4

Streamer Propagation

After initiation, a streamer will propagate under the influence of an external electric field augmented by its self-generated field, as already discussed in Section 1.2.2. To sustain the extension of the plasma channel by impact ionization in the high-field zone, enough free electrons need to be present there. In negative streamers, the electrons drift from the ionized region in the direction of streamer propagation and reach the high-field zone. However, in positive streamers, the electrons cannot come from the streamer itself. Therefore, for positive streamer propagation, “fresh” electrons are needed in front of the streamer head. The possible sources of these free electrons are discussed below.

As was discussed in Section 1.1.5, the positive charges indicated in Figure 1.3 will mainly consist of positive molecular ions and the negative charges indicated in the streamer tails in air in Figure 1.3 will be negative molecular oxygen ions, limiting the total conductivity. Therefore, streamers in pure nitrogen can become longer than those in air under similar conditions as less electron attachment occurs if current flow from behind is required. The negative charges in the streamer head, as well as the moving charges in front of the streamer heads, will be mostly free electrons.

Owing to the electric screening layer around the curved streamer head, the electric field ahead of it is usually much higher than the external or background field.

1.2.4.1 Electron Sources for Positive Streamers

Positive streamers need a constant source of free electrons in front of them in order to propagate. Because of the electronegativity of molecular oxygen, free electrons in air quickly attach to oxygen by Eqs. (1.4) and (1.5) if the electric field is below $\sim 30 \text{ kV cm}^{-1}$. If this is the case, a high field is needed to detach the electrons so that they can be accelerated. The exact level of the detachment field depends on the vibrational excitation of the molecule. According to Pancheshnyi [88] and Wormeester *et al.* [89], a good value of the instant detachment field under standard conditions in air is 38 kV cm^{-1} .

Photoionization In most streamer models, air is the medium and the major source of electrons in front of the streamer head is taken as photoionization. In air, photoionization occurs when a UV photon in the 98–102.5 nm range, emitted by an excited nitrogen molecule, ionizes an oxygen molecule, thereby producing a free electron.



As the emitted photon can ionize an oxygen molecule some distance away from its origin, this is a nonlocal effect, therefore, excited nitrogen molecules in the streamer head can create free electrons in front of the streamer head (as well as

in other places around the streamer head). The average distance that a UV photon can travel depends on the density of the absorbing species, oxygen in this case. In atmospheric pressure air under standard conditions, this distance will be about 1.3 mm [90].

Background Ionization Besides photoionization, there is another source that can provide free electrons in front of a positive streamer head: background ionization. Background ionization is ionization that is already present in the gas before the streamer starts, or at least, it is not produced by the streamer. It can have different sources. In ambient air, radioactive compounds (e.g., radon) from building materials and cosmic rays are the most important sources of background ionization. They lead to a natural background ionization level of 10^9 – 10^{10} m^{-3} at the ground level (Pancheshnyi [88]).

Another source of background ionization can be leftover ionization from previous discharges. This is especially important in repetitive discharge types such as DC corona discharges or repetitive pulsed discharges. Already at a slow repetition rate of about 1 Hz, leftover charges can lead to background ionization densities of the order of 10^{11} m^{-3} . Background ionization can also be created by external UV radiation sources, X-ray sources, addition of radioactive compounds to the gas or surfaces, electron or ion beam injection, and more.

Independent of the source of background ionization, in air, the created electrons will always quickly be bound by oxygen. This means that they will have to be detached by the high field of the streamer before they can be accelerated and form avalanches.

1.2.5

Initiation Cloud, Primary, Secondary, and Late Streamers

Recent imaging with high spatial and temporal resolution has shown how a streamer tree starts from a needle electrode, which in most cases is positively charged [91–93]. The discharge starts with a small ball of light around the needle tip that was called the *initiation cloud*. This ball expands and forms a shell; this shell can be interpreted as a radially expanding ionization front, and in the case of a negative needle tip in air, its maximal radius fits the theoretical estimates well [93]. For positive voltages, it has been verified that the size l of the initiation cloud scales with gas density n_0 according to the similarity laws ($l \propto 1/n_0$) but it also depends on gas composition and, of course, on the applied voltage. For example, in air, the initiation cloud is much larger (up to a factor 10 or more) than in pure nitrogen [91]. In fact, what on time integrated images of the discharge seems like a light emitting cloud is in fact often a smaller cloud that transforms into a thin expanding shell.

Eventually, the expanding shell breaks up into multiple streamer channels, except when the gap is so small that the initiation cloud extends into roughly half the gap distance; in that case, it usually destabilizes into one channel only. These first streamers emerging from the initiation cloud are called *primary streamers*. Example

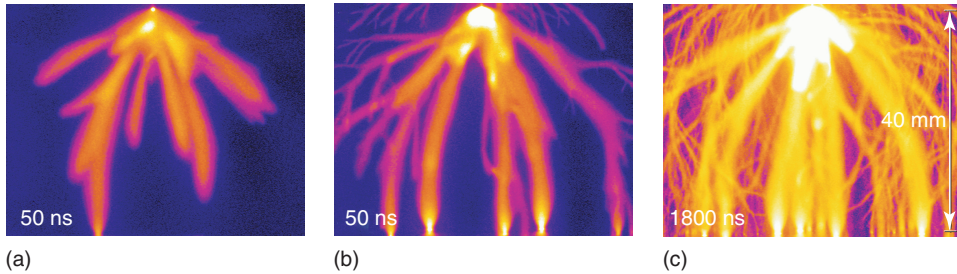


Figure 1.4 Streamer discharges in a 40 mm gap in atmospheric air with a 54 kV pulse, 30 ns risetime, and half-width of about 70 ns. The images are acquired with short (a,b) and long (c) exposure times.

The exact image start delay is varied between (a) and (b) (exact values unknown). (Source: Images by Tanja Briels, originally published in Figure 6 of Ref. [77].)

of such streamers are shown in Figure 1.4a,b. For long gaps, low voltages, or short pulse durations, the primary streamers often do not reach the other side and extinguish somewhere between the electrodes.

Briels *et al.* [77, 94] characterize different streamer types with very different diameters and velocities, although they realize and later show [78] that there is no phase transition between these types. For voltages between 5 and 95 kV, the streamer diameters vary by more than an order of magnitude and the velocities by almost 2 orders of magnitude. The relation between velocity and diameter is discussed in [79, 81]. The streamers with minimal diameter (the so-called minimal streamers) are never seen to branch. This minimal diameter depends on density, roughly in agreement with the similarity laws [3], but it does not depend on the background field or other pulse parameters. This concept was proposed by Ebert *et al.* [95]. The thick streamers grow only if the voltage rises sufficiently fast. Only then there is sufficient voltage initially on the pointed electrode to develop a very wide ionization cloud that can eject fat streamers.

After the primary streamer, more light-emitting discharge phenomena can occur. If the same streamer channels reilluminate rather immediately, one speaks of a secondary streamer, while if a streamer follows a different track at some later time, one speaks of a late streamer.

Secondary streamers have been described, for example, by Marode [96], Sigmond [97], Ono and Oda [98], or Winands *et al.* [5]. Sigmond remarks that moving secondary streamer fronts in centimeter-scale gaps in atmospheric air does not perturb the smoothly decaying streamer current and that they are only reported in air. Ono and Oda [98] have compared primary and secondary streamers; they were created in air in a needles-to-plane geometry with gaps of 13 mm length and voltages of 13–37 kV (compare with the 37–77 mm, 25–45 kV wire plane discharge of Winands *et al.*). They observe that emission from the FNS of N_2^+ (391.4 nm) is only observed in primary streamers and not in secondary streamers. This is attributed to the fact that electron energies required for propagation of primary streamers are higher than those for secondary streamers as primary streamers

have to create ionization, while secondary streamers propagate along the ionized channel created by the primary streamers. Furthermore, they find that secondary streamers only occur at higher voltages (15 kV in air and 20 kV in pure nitrogen). van Heesch *et al.* [1] found that the O^* radical yield from primary streamers is up to two times higher than that from secondary streamers. They explain this by higher local electric fields and electron energies in the primary streamers.

The literature presents different suggestions for the physical mechanism of secondary streamers. Marode [96] suggests that secondary streamers correspond to a moving equivalent of the positive column of a glow discharge. Sigmond [97] suggests that the ionized column created after the primary streamer has crossed the gap decays into one region with high and another region with low electric field due to an attachment instability. The electrodynamic consistency of these calculations is under examination at present. A different mechanism is suggested by recent simulations of Liu [99] and Luque and Ebert [80]. They find that inside a streamer that requires a growing charge in its tip – because it accelerates and expands or because it propagates into a region with higher gas density – a secondary ionization wave can set in, and that the electric field inside this wave reaches approximately the breakdown field. This process can set in before the primary streamer has reached an electrode. We note that in the experiments of Winands *et al.* [5] where long secondary streamers were observed, the primary streamers were accelerating and expanding as well, just like in the simulations of Liu.

A third streamer category, besides primary or secondary streamers, is the so-called late streamers. They occur only for long enough pulses and are, in fact, the primary streamers that either start later than the dominant streamers or are so slow that they seem to have started later. Late streamers propagate along completely different paths than the other (primary) streamers before them. They are often very thin, which is related to their slow propagation velocity (see, e.g., Briels *et al.* [78]). In most cases, they do not appear from the sharp electrode tip itself but instead from the (less sharp) edges of the electrode or electrode holder because the tip is already screened by a glow region and therefore no longer enhances the electric field sufficiently. Examples of these late streamers are visible in Figure 1.4b,c. In Figure 1.4b, the late streamers have just started and are visible on the top of the image. In Figure 1.4c, a much longer camera exposure is used. Therefore the primary streamers are now overexposed as their secondary and glow phase is also included in this exposure. However, many (thin) late streamers are clearly visible crisscrossing all corners of the image.

1.2.6

Streamer Branching and Interaction

Most streamer discharges contain more than one streamer channel. Therefore, interactions between streamers are important when studying streamer behavior. One important aspect is streamer branching where one streamer channel splits into two (or more) channels. Other interactions are attraction and repulsion of streamer channels. Furthermore, neighboring channels influence each others

field configuration. If attraction occurs, this may lead to streamer merging or (re-)connection. Discussion and measurements regarding streamer merging and (re-)connection are given by Nijdam *et al.* [100, 101].

Branching is observed in most streamer discharges, except when the gap is so short that the streamer has reached the other side before it has branched. Furthermore, streamers of minimal diameter (so-called minimal streamers, see below) also do not branch but eventually extinguish. This is the main argument why streamer discharges are never real fractals.

The mechanism of streamer branching has been under investigation for quite a long time now. It is certainly due to a Laplacian instability of the thin space charge layer visible in Figures 1.2 and 1.3; this instability bears strong mathematical similarities with viscous fingering [102]. For a recent review of the analytical, numerical, and experimental results, we refer to [71]. The Laplacian instability can actually set in without any stochastic effects [102, 103]. However, the branching instability can be accelerated by electron density fluctuations in the lowly ionized region ahead of the streamer [104]; these fluctuations are due to the discrete quantum nature of the electrons. Indeed, these fully three-dimensional recent simulations for positive streamers in air (with the standard photo-ionization model) show a ratio of streamer branching length to streamer diameter similar to that obtained in experiments [91, 100].

The acceleration of branching through electron density fluctuations is consistent with older concepts, which can be traced back to Raether [86] and Loeb and Meek in 1940 [105]. However, in these older sketches, the fact that the streamer has to develop a thin space charge layer before it can destabilize was missed. The older concept that can be found in many books emphasizes the spatially well-separated avalanches ahead of the streamer as direct precursors of different branches. Such avalanches have now indeed been seen in very pure gases [89, 106]. However, the photoionization density in air is much too large to create individual avalanches [107].

van Veldhuizen and Rutgers [108] have experimentally investigated streamer branching in argon and ambient air for different discharge geometries and pulse characteristics. They find that streamers in a point-wire discharge branch about 10 times more often (in the middle of the gap) than in a discharge between a plane with a protrusion and another plane.

A very different branching mechanism is branching at macroscopic inhomogeneities such as bubbles (for streamers in liquids). This mechanism was recently described in detail by Babaeva and Kushner [109].

A proper understanding of streamer branching, on the one hand, and streamer thickness and efficiency, on the other hand, is required to understand which volume fraction of gas is being processed in a streamer corona reactor. The streamer interaction mechanisms discussed above are an important ingredient for building models of a complete streamer discharge. However, a complete model based on measurements or theoretical understanding of the microscopic processes is not yet available. There are a number of models for streamer trees that start from phenomenological assumptions of streamer channel properties as a whole.

All currently available models neglect the large variation of streamer diameters and velocities in pulsed corona reactors. The first phenomenological model for a complete discharge tree was proposed by Niemeyer *et al.* [110]; it approximates sliding surface discharges and creates fractal structures. This model includes streamer branching in a purely phenomenological manner and assumes that all streamers are equal and that the interior is completely screened from the electric field. Since then, a number of authors have developed this model further, in chemical physics, geophysics [111], and electrical engineering [112]. At present, the challenge lies in extending such models to all recently identified microscopic ingredients such as branching statistics, streamer diameters and velocities, and interior electric fields coupled to the external circuit.

1.3

Glow Discharges at Higher Pressures

1.3.1

Introduction

The classic low-pressure glow discharge has been studied extensively for several decades. The discharge is typically produced in a low-pressure (order of 1 mbar) noble gas between two electrodes that are separated from 1 cm up to 1 m. The light emission pattern of a low-pressure glow discharge is described in all standard books [113] and includes a cathode glow, cathode dark space, negative glow, Faraday dark space, the positive column, the anode dark space, and the anode glow.

The sheath region of a glow discharge has a high electric field because of charge separation between fast electrons and slow positive ions (creating the so-called cathode fall). The fast electrons emitted by the cathode and accelerated by the high field multiply by impact ionization on the sheath edge. In many glow discharges, most space between the electrodes is occupied by the positive column, a region with a relatively low, constant electric field. See also Šijacic and Ebert [114] for a detailed description and numerical model of the Townsend to glow discharge transition. In their one-dimensional model (equivalent to a plate–plate discharge), they found that depending on $p \cdot d$ (pressure times distance) and the secondary emission coefficient of the cathode γ , the transition can occur according to the subcritical behavior described in books (with a negative current–voltage characteristic (CVC) from Townsend to glow) or for smaller values of $p \cdot d$, it can also behave supercritical or have some intermediate “mixed” behavior.

In spite of the fact that it is easy to produce glow discharges at low pressure (applying typically a few hundred volts DC), with increasing pressure, the glow discharge has the tendency to become unstable and constrict: a glow-to-spark transition occurs. Thus, at atmospheric pressure, it is necessary to use special geometries, electrodes, or excitation methods to obtain diffuse glow discharges. Spark/arc formation is a restriction for the generation conditions of nonthermal (cold) atmospheric pressure plasmas in general.

High-pressure glow discharges have been studied for several years because they are scalable to large areas while remaining relatively uniform. This is especially interesting for surface interactions under controlled conditions without the necessity of vacuum equipment. Studies of atmospheric pressure glow discharges (APGDs) go back to von Engel *et al.* [115]. High-pressure glow discharges and also the instabilities that occur have been studied in the context of the construction of lasers [113]. More recently, these discharges are produced to obtain homogeneous treatment of materials and large-volume homogeneous discharges [116, 117].

A possibility to prevent the direct transition from a Townsend to a filamentary discharge is increasing the preionization in the gas [84]. Basically, the electrical field is reduced by the interaction of the avalanches, which does not allow the Meek criterion to be reached. The avalanche-to-streamer transition and the start of filamentation of the discharge is more suppressed.

1.3.2

Properties

It must be noted that several authors use the label glow discharge, in general, for a discharge that looks homogeneous to the naked eye. A more strict use of the term *glow discharge* is often appropriate, especially because discharges of a filamentary nature, such as certain DBD discharges, can look very diffuse when time averaged, while the properties and chemistry can be quite different from diffuse discharges. In spite of several differences between the low-pressure glow discharge and APGD, there are several similarities that motivate the use of same label glow discharge at atmospheric pressure also.

The similarities with low-pressure glow discharges include the following:

- The reduced current density (J/n_0^2) is independent of density (or pressure) and applied voltage.
- The characteristic light emission pattern of the glow discharges.
- There is constant electrical field in the positive column.
- The discharge voltage is independent of the current when corrected for the temperature rise, constriction of the positive column, and current dependence of the cathode–anode voltage drop.
- The electron temperature is much higher than the gas temperature.
- The glow discharge operates at the Stoletov point; that is, the thickness of the cathode fall region is adjusted so that the conditions to operate in the minimum of the Paschen curve are reached.
- The burning voltage and cathode voltage drop is significantly larger than in the case of arc discharges.

The main differences with low-pressure discharges are the following:

- The dimensions of the characteristic light emission pattern of the glow discharges scale (inversely) with pressure and are considerably smaller (typically tens or hundreds of meters at atmospheric pressure instead of centimeters at millibar pressure).

- Owing to the high pressure, gas heating can be considerable up to a few thousand kelvin while most low-pressure glows are close to room temperature.
- Owing to gas heating, scaling laws always need to be written as a function of density and not pressure, as is mostly done in the old literature (for low-pressure discharges).
- At low pressure, the electron losses are dominated by diffusion, while in the high-pressure case, due to the high collisionality bulk processes (such as dissociative electron-ion recombination) become important.
- The sheath is highly collisional at atmospheric pressure, which means that the ion energies impacting the electrode are considerably smaller than at low pressure.

The electron density of diffuse APGDs is estimated to be in the range 10^{17} – 10^{19} m^{-3} . This is too low for accurate line-broadening measurements. Only few measurements exist that are based on microwave absorption [118] and millimeter wave interferometry [119]. They give values of 4 – 7×10^{17} and 8×10^{18} m^{-3} , respectively. Other values are often derived from modeling or estimates from current densities and are not very accurate. Gas temperatures range from room temperature up to 3000 K [56, 120, 121]. The electron energy distribution is highly non-Boltzmann. High-energy electrons are produced in the cathode region, penetrate in the bulk, and sustain the discharge. The electron energy in the bulk is of course much lower (often the values of an effective electron temperature of 1–5 eV circulate in the literature), but often, a high-energy component originating from the cathode region in small electrode gaps is present [122].

1.3.3

Studies

Standard glow discharges have to be stabilized with a negative feedback, for example, by including a resistor in series. The series resistor can prevent current runaway as the resistor causes the voltage across the discharge gap to decrease with increasing current for constant applied voltage. Similar behavior can be obtained by using a capacitor or inductance in series with the discharge gap. The latter has been shown by Aldea *et al.* [123], who used it to stabilize large area APGDs for material treatment applications.

The lumped resistor approach can work, but using a resistive electrode or a dielectric barrier between the electrodes causes a distributed resistor or capacitor, which can even enhance the diffusivity of the discharge. Atmospheric pressure glow discharges stabilized by resistive electrodes are studied by Laroussi *et al.* [124]. Also, water electrodes (which are, of course, resistive in nature) are used to generate glow discharges, as has been studied by Andre *et al.* [125], Lu and Laroussi [126], and Bruggeman *et al.* [127]. Bruggeman *et al.* have shown that in the case of a liquid electrode, there is a significant polarity effect. In the case of a water cathode, the discharge is filamentary close to the cathode because of instabilities of the liquid surface caused by the strong electrical field in the cathode layer. When the discharge is generated between a liquid anode and a metal cathode, a diffuse glow

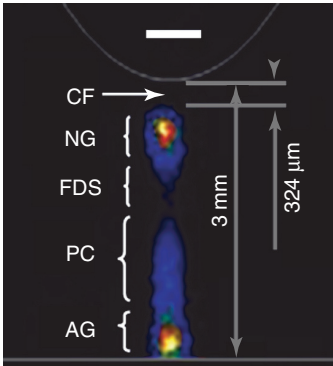


Figure 1.5 Example of an atmospheric pressure air glow discharge in a metal pin (top) water electrode (bottom) geometry. The typical structures of the low-pressure glow discharge are clearly visible, although on a sub-millimeter scale. (CF) cathode fall; (NG) negative glow; (FDS) Faraday dark space; (PC) positive column; (AG) anode glow. (Source: Taken with permission from Ref. [20].)

is observed, which has the same characteristic emission pattern as the low-pressure discharge, but on a (sub) millimeter length scale [120] (Figure 1.5). Diffuse DBD discharges have been investigated by many authors. Nonetheless, in this case, a diffuse glow discharge is not always found. The discharge often looks diffuse but consists of filamentary microdischarges, as will be discussed in more detail in the section 1.4 on DBD discharges. For higher frequencies (hundreds of kilohertz) and in gases such as He and N₂, diffuse glow discharges can be obtained [128, 129]. Note that sometimes the addition of a trace gas turns a filamentary discharge into a diffuse discharge, which indicates a clear dependence of filamentation on the chemistry of a discharge. Massines *et al.* also investigated low current discharges without the development of space charge in DBD configurations in the context of material treatment. This Townsend mode is a low-intensity diffuse plasma, but only for higher current densities and after the development of space charge, glow discharge structure with significant emission in the cathode region (negative glow) is observed. An example of a diffuse and a filamentary discharge in a parallel plate DBD geometry is shown in Figure 1.6.

DC glow and microglow discharges between two metal electrodes were investigated by Staack *et al.* [121]. The microglow discharges remain stable because of the high surface–volume ratio and thus efficient heat removal. For discharges on a micrometer scale, the positive column is not present. This increases the stability of the discharge, as well as a positive column has the tendency to contract, for example, due to significant heating and a heating ionization instability. That is, for a fixed E field E/n_0 increases with increasing temperature, which means that the ionization rate, and consequently, the electrical conductivity and the heating, also increases. This again leads to an increase of E/n_0 and consequently runaway behavior. Large-scale glow discharges have the tendency to contract radially.

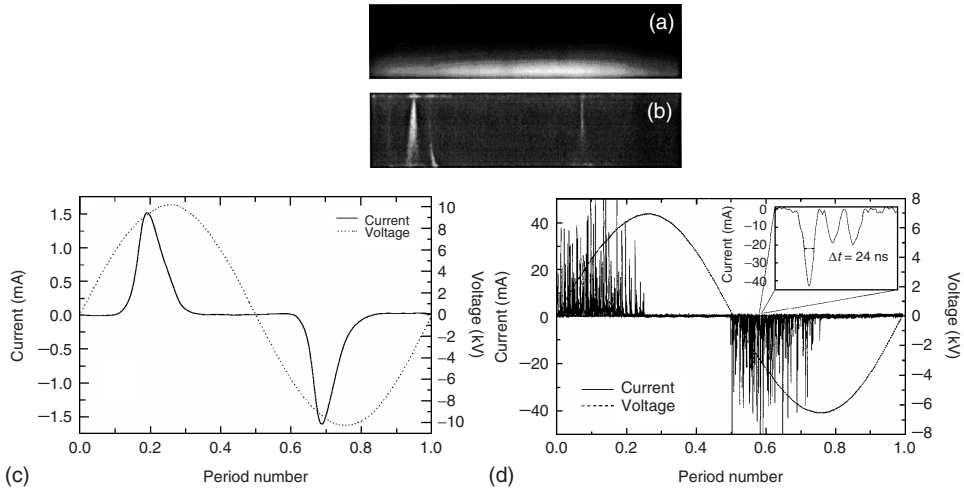


Figure 1.6 The glow mode (a) and the filamentary (micro-discharge) mode (b) in a parallel plate dielectric barrier. The corresponding current (c) and voltage (d) waveforms are shown as well. It is clearly visible

that in the filamentary mode, the current pulses of microdischarges can be observed, while in the glow mode, there is a broad current peak for every voltage cycle. (Source: Taken with permission from Ref. [130].)

The CVC of microglow discharges can also be positive in contrast with most other glow discharges. This is in agreement with [114] where the CVC of one-dimensional glow discharges is calculated in the simplest possible model for different gap lengths, and it is found that in short gaps, there is no falling CVC, that is, no negative differential conductivity (NDC), in agreement with early measurements. Raizer *et al.* [131] gives a small correction to [114]. The calculation is done assuming a constant γ of secondary emission.

Šijacic *et al.* [132–134] treat a system where a planar discharge (between Townsend and glow) is sandwiched with a planar high-ohmic semiconductor between planar electrodes to which a DC voltage is supplied. It is believed that a negative differential conductivity would be necessary for spontaneous oscillations [135], but that is not true – a falling CVC of the discharge in the gap as a whole should not be confused with a local NDC. In [132, 133], we analyze the oscillations in [134] and also spatiotemporal patterns.

The Loughborough group has studied RF APGDs in He in a parallel plate metal electrode geometry [136]. It is interesting that this discharge, just like at low pressure, operates in two modes, the alpha and the gamma mode. In the alpha mode, the discharge is sustained by bulk ionization, while in the gamma mode, the discharge is sustained by the electrons generated at the cathode [137]. The discharge often has the tendency to contract radially in the gamma mode.

Several microplasmas can also be categorized as glow discharges. Many different configurations exist, and the reader is referred for a thorough review to [27]. The hollow cathode discharges, for example, can operate in a glow mode at low

currents and in an abnormal glow mode when the entire cathode electrode area is covered. In the abnormal glow discharge, the voltage increases with current as the increase in electrode area cannot compensate anymore for the current increases at constant discharge voltage. For microdischarges, the electron density can be of the order of 10^{21} m^{-3} or even higher. Gas temperatures are often 1000 K or larger. Microdischarges are very efficient for producing excimer light.

Atmospheric pressure jets, which are now very popular for biomedical-oriented research, are also often considered to be microplasmas. These plasmas operate at a lower gas temperature. They are mostly constructed in a DBD configuration (see further). In addition, the air flow, and often the He carrier gas, causes an even larger reduction in temperature compared to other typical microplasmas.

The groups of Akishev and Leys investigated the stabilization of high-current negative-glow corona discharges. It is found that with a gas flow of the order of 10 m s^{-1} the transition from the glow to spark can be postponed to larger currents [138, 139]. In this extended operation range, the discharge deviates from the CVC of a negative corona ($I = kV(V - V_0)$) due to the growing importance of space charge. With flow stabilization, it is possible to produce large-volume plasmas in centimeter gaps.

From the point of view of diagnostics, interesting work has been done on the chemical activity of nanosecond-pulsed discharges (which can also be of the glow type) by Stancu *et al.* [58]. Optical studies of these discharges have been done, for example, by Bruggeman *et al.* [120], Laux *et al.* [53], Machala *et al.* [140], and Schulz-von der Gathen *et al.* [141]. More recently, the ion flux to the electrodes of an RF-excited APGD in He–H₂O has also been studied [62]. However, a lot of these results remain disperse and several open questions remain, especially for discharges operating in gas mixtures containing molecular gases, which is typically the case for applications. These open questions have been partly attacked by modeling such as is intensively made at the groups from, for example, Loughborough University [122] and Queens University, Belfast [142, 143]. Recently, attempts to study an extensive chemistry in these discharges with a zero-dimensional model are published by Liu *et al.* for He–O₂ and He–H₂O diffuse-glow RF discharges [144, 145].

1.3.4

Instabilities

Glow discharge instabilities can occur at the anode [146], at the cathode [147–149], and in the gap [150, 151]. In order to get a glow-to-spark transition, a certain amount of energy needs to be dissipated in the discharge during the glow phase [152]. In cases when the constriction starts at the cathode, this is believed to be in the cathode fall region. It is clear from the different locations where the instability starts that the instabilities are strongly influenced by the exact discharge geometry and electrode properties. Suleebka *et al.* [153] studied constriction of a high-pressure glow discharge in hydrogen and concluded that the electrode history and the amplitude of the overvoltage significantly alter the initial location of the constriction. In the first series of experiments, they found that the constriction of

the glow always started at the cathode. When the electrodes become conditioned (after formation of an oxide layer), the constriction is initiated at the anode, in the midgap, and again at the cathode with increasing overvoltages. Recently, the glow-to-spark-transition is investigated in a metal pin–water electrode geometry, which indicated that in the case of low conductivity of the water electrode broadened sparks are observed [151]. This is a nice example of the stabilization of resistive electrodes on the constriction of diffuse glow discharges even after a contraction occurred in the bulk of the discharge.

Recently, Pai *et al.* [154] investigated nanosecond-pulsed atmospheric pressure discharges that can occur in a corona, glow, and spark mode. The glow-to-spark transition has been described by the thermal instability mechanism. It must be mentioned that no general criterion for the contraction of APGDs exists.

1.4

Dielectric Barrier and Surface Discharges

1.4.1

Basic Geometries

Electric discharges in air under ambient conditions have a strong tendency to develop instabilities. These instabilities can develop in space, that is, streamers or filaments, and λ also in temperature, that is, sparks or arcs. Both effects are undesired if one wants to use a volume discharge for chemical conversions. Sparks can be suppressed relatively easily by limiting the current. One way to limit the current is to use a series resistance. This can be done by adding a resistor in the power supply lead or by using a semiconductor for electrode material. A disadvantage of the resistive method is that it leads to loss of electrical energy that is converted into heat. A second way to limit the current is the use of dielectric barriers. The breakdown field strength of a dielectric can be up to hundred times higher than that of air. Therefore, when a streamer reaches the dielectric layer on top of the electrode it will extinguish. Figure 1.7a–c shows the basic shape with two flat electrodes and one or two dielectric barriers. Coaxial shapes, as shown in Figure 1.7d, are very common in ozonizers and other cases of gas treatment.

In the early days, the common dielectric material was glass, which could be the reason why cylinders were often used. Large systems are made with hundreds of long cylinders in parallel [51]. Ozonizers with a capacity of 100 kg O₃ per h have been made this way [4]. Nowadays plastics and ceramics are more common. Sufficient breakdown strength of the dielectric layer is mandatory. But a thicker layer requires a higher voltage, so a compromise must be made here. The dielectric material must be extremely free of voids to avoid damage in the long term. As in high-voltage cable, partial discharges are initiated in voids, which lead to degradation of the dielectric [155]. It can take up to many years before damage occurs. Therefore this effect is mostly unnoticed in laboratory experiments but crucial for robustness of commercial applications.

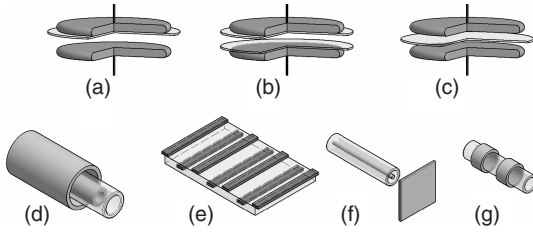


Figure 1.7 Dielectric barrier discharge configurations: (a–c) plane barriers, mostly used in research, (d) coaxial design, often used in ozonizers, (e) (partly) buried electrodes for surface discharge, and (f,g) plasma jets as used in, for example, biomedical applications.

Barrier discharges work best with an electrode separation of a few millimeters. The discharge becomes too inhomogeneous with larger gaps. A good example of this effect is shown in [156]. The spatial nonuniformities of the barrier discharge are a subject of study even now. Recent work on this pattern formation can be found in [157]. In the 1990s, research was begun on how to avoid the inhomogeneities. A good explanation on how to obtain the Townsend, glow, or filamentary discharge was given by Massines and Gouda [116] (Figure 1.6). The transition of the glow discharge into filaments can be avoided with electronic stabilization, as demonstrated by Aldea *et al.* [123]. By now, APGDs have been achieved in barrier discharges in several gases [16, 17].

Alternative geometries have gained a lot of interest in the recent years. The first are dielectric sheaths with electrodes on the top or inside; an example is given in Figure 1.7e where the electrodes are alternatively inside and on the top of the dielectric. All electrodes inside go to one connector of the power supply and all electrodes on the top to the other. The discharge develops from the electrodes on the top over the dielectric surface. A different layout is shown in Figure 1.8. This is a photo of a stack of plastic plates covered on both sides with meshes that are connected to a transformer. The discharge develops at the mesh wires. Very large systems are easily made with this method at relatively low cost. Geometries with electrodes buried in the dielectric were pioneered already in the 1980s by Masuda *et al.* [158], and many alternatives exist nowadays [16, 18]. A nice example of this type of discharge is the plasma display panel (PDP) as used in televisions [159]. Panasonic claims to have made the world's largest plasma TV with a diagonal of 152 in., that is, almost 4 m.

An even newer concept is the cold atmospheric pressure (CAP) plasma jet, two possible shapes are shown in Figure 1.7f,g. This type of plasma source is made for local treatment and is especially popular in biomedical applications [160]. An important aspect is that the gas stays close to room temperature. The electric power consumption ranges from far below 1 W to about 10 W [161], in this case with 13.56 MHz excitation frequency and electrode configuration of Figure 1.7f. Figure 1.9 shows a photo of an RF plasma jet made at the Technische Universiteit, Eindhoven. It has a 1 mm pin electrode inside a 2-mm glass tube with a helium

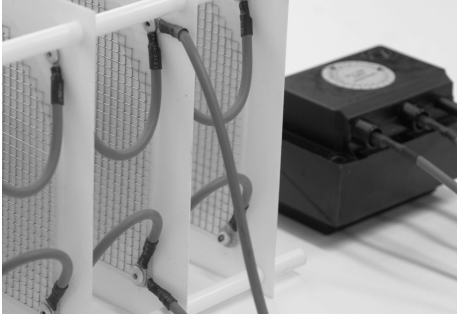


Figure 1.8 PlasmaNorm[®] demonstration unit, that is, a dielectric barrier discharge made from plastic sheets with a metal mesh on both sides. The power supply is a 50 Hz high-voltage transformer. (Source: Courtesy of Circlair Benelux BV.)

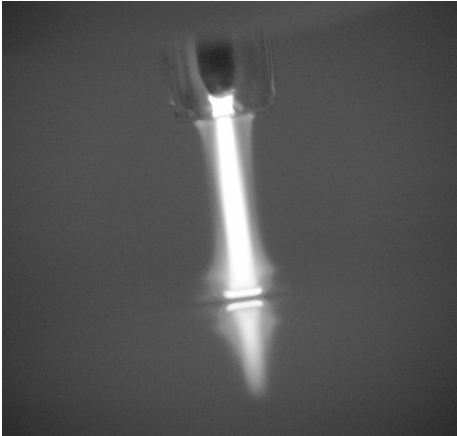


Figure 1.9 RF helium plasma jet hitting a glass substrate. (Source: Photo: Sven Hofman, TU/e.)

flow of 1 l min^{-1} . The power consumption by the plasma is 1 W. Lower frequencies are also used, for example, in the kilohertz range [162], mostly with ring electrodes as in Figure 1.7g. Even microwave frequencies of 2.54 GHz [28] are applied in coaxial configurations where the outer cylinder is metal. The microwave power can be up to tens of watts, which will lead to considerable gas heating.

Recent reviews on plasmas for biomedical applications are made by Ehlbeck *et al.* [163] and Lee *et al.* [164]. The plasma jet geometry is also used in combination with nanosecond pulses; in this way, the so-called plasma bullets are created. This method was probably first discussed by Laroussi and Lu [24]; a detailed study is reported by Jarrige *et al.* [165].

1.4.2

Main Properties

The conventional barrier discharge as shown in Figure 1.7a–c is a mixture of a volume and a surface discharge. The first free electron that initiates an avalanche is most likely in the volume. When the applied field is high enough, this avalanche develops into a streamer that travels toward both electrodes since this field is homogeneous. A gap distance of the order of 1 mm is already sufficiently large at a pressure of 1 bar, which is the standard in practically all applications. Most barrier discharges are excited with sine waves, so the streamer velocities will be near the minimum value of 10^5 m s^{-1} [78]. This implies that a streamer reaches the electrodes within 10 ns. After that it can continue across the surface of the dielectric as long as the field strength is high enough. However, the streamer heads deposit charge on the surface where they land and this charge counteracts the applied field. So the discharge extinguishes naturally, and there is no risk for breakdown into a spark as long as the dielectric material is unimpaired. This is the main advantage of the barrier discharge.

The charges can stay on the surface for many seconds, that is, much longer than the repetition time of the applied voltage pulses, which is in the millisecond range. Therefore, a second pulse of the same polarity will still notice counteraction of the surface charge on the dielectric and the discharge will not ignite again. For this reason, barrier discharges are operated with alternating voltage sine waves so that the applied field adds up to the space charge field, which makes it even easier for a new discharge to develop. The frequencies used mostly range from 50 Hz to 100 kHz, but frequencies up to many megahertz are encountered especially in miniature versions, the so-called microdischarges [26]. This name is used, however, for many different geometries and does not always refer to discharges on the micrometer scale.

The question arises how barrier discharges differ from other cold atmospheric plasmas and do they have typical characteristics that make them suitable for certain applications. Table 1.1 gives a coarse overview on these items.

An important question is what makes a certain discharge suitable for a certain application? From Table 1.1, one can conclude that it is basically the shape that is determining: large gaps to treat gases and small gaps and jets for surface treatment. But now the question arises whether or not there are more fundamental differences between these two types of discharges. In the early years of 2D streamer calculations, there was a general idea that corona discharges had a higher electron energy than barrier discharges [8, 34, 166–169]. Numbers mentioned for average electron energies in the streamer heads were 5–15 eV for coronas and 2–6 eV for barriers. The main difference between both discharges is the shape of the applied electric field. In coronas, it is very high near the sharp electrode and below inception in the bulk of the gas; in barrier discharges, the field is more or less homogeneous and above inception in the whole gap.

More recent simulations and experiments (such as those discussed in Section 1.2.2 also) support these general conclusions. From experiments it was

found that the T_e and n_e of filamentary DBD discharges, which normally operate close to room temperature, are 1–2 eV and 10^{20} – 10^{22} m⁻³, respectively [170–172]. This is not exactly the same as the older calculations but still supports its general conclusions that in a DBD discharge the electron temperature is lower but the electron density is higher than in a corona discharge. However, in combination with the wide range of circumstances of all discharges being involved, general conclusions cannot be drawn on how to select a certain discharge for a specific application. For the time being, this will remain an empirical process.

1.4.3

Surface Discharges and Packed Beds

As said before, a barrier discharge can be a combination of a volume discharge and a surface discharge or it is only a surface discharge. Specific geometries are made to provoke only surface discharges, such as shown in Figure 1.7e. Similar to barrier discharges, the surface discharge can appear in the shape of filaments or as a homogeneous glow. The surface discharge is also known from high-voltage equipment where it is definitely undesired because it can lead to serious damage [173]. It is generally known that flashover occurs more easily over a surface than through a volume with gas under ambient conditions. The condition of the surface plays a major role here: scratches, dirt, or moisture facilitate the breakdown process. However, only a few fundamental processes that can cause this difference are known: electric charges that are somehow deposited can change the applied field strength [37] and electrons can be released from the surface either by ions [38] or by UV photons [39]. Measurements that reveal differences between surface and volume discharge are very limited. An example is the point-plane geometry studied by Sobota *et al.*, where a dielectric is placed at different distances from the point [174, 175]. An interesting result is that the streamer across the dielectric propagates roughly two times faster than the streamer through the bulk gas, which is argon in this case. Measurements in air were performed by Morales *et al.* [176]; here the influence of pulse rise time and UV radiation was studied. The propagation velocities along a surface in air were measured by Deng *et al.* [177]. Their values are lower than the ones found for argon, the much slower voltage pulse rise time is probably an important factor here. A very interesting aspect of the surface discharge is that surfaces of birefringent material give information of the local electric field strength and the surface charge density. Bismuth germanium oxide crystals are generally used for this purpose, the method is described in detail by Gegot *et al.* [178]. Tanaka *et al.* [179] have used this method to obtain 2D profiles of charge and potential on the surface. They found that the horizontal component of the electric field reaches a maximum on the tip of the streamer and is derived to be 15–30 kV cm⁻¹, that is, equivalent to ~2–3 eV electron energy. This low value is in agreement with the idea that the surface makes it easier for the streamer tip to propagate. Numerical calculations are very difficult in this area because quantitative data on the aforementioned fundamental processes are not available and because the surface streamer process is inherently 3D. 3D gas phase streamer simulations

are now becoming available [74, 82, 83, 90], so surface streamer simulations might follow soon.

Packed bed barrier discharges mostly use beads of dielectric material to get a large surface area for enhancement of chemical reactions. These beads can be covered with a catalyst [180]. It is usually assumed that the beads are covered with a surface discharge. This situation is more complex than the planar surface discharge and it appears that no detailed studies of the plasma properties and the plasma chemical kinetics are available.

1.4.4

Applications of Barrier Discharges

The coaxial electrode configuration of Figure 1.7d was first described by Werner Siemens in 1857 [181]. This opened the way for stable and large-scale production of ozone. In 1886, De Meritens discovered that ozone could destroy microorganisms, and in 1906, the city of Nice had already introduced ozone treatment for drinking water. Nowadays, ozone technology is mature, a lot of information can be found in books [182–184] and in a fully devoted journal [185]. Practically all this ozone is made by barrier discharges.

An important aspect of an industrial ozone generator is its yield, usually expressed in grams per kilowatt-hour. A calculation based on the enthalpy of formation shows that a 100% efficient reactor would produce 1.22 kg kWh^{-1} . Probably, the best laboratory result for ozone production in air is still 180 g kWh^{-1} as reported by Masuda *et al.* [158]. For a commercial equipment, where a lot of emphasis is put on lifetime and reliability of the equipment, the production is usually in the range of $1\text{--}50 \text{ g kWh}^{-1}$. A pilot plant for flue gas cleaning based on pulsed corona achieved 45 and 60 g kWh^{-1} [186] for pulses with high and low energy, respectively. This demonstrates again that corona and barrier discharges seem to perform equally in terms of chemical yield, although there are indications that the efficiency of nanosecond-pulsed corona discharges can be higher [1]. A new and interesting method for ozone production is the use of xenon excimer lamps [11]. Such lamps very efficiently produce light with a wavelength of 172 nm. This light dissociates oxygen, and as claimed by Salvermoser: “A 172 nm VUV ozone generator operating in a cold environment with ambient air as a feed gas could easily produce 2 wt% of ozone with a wall plug ozone yield of 150 g/kWh without any NO_x -contamination present” [11]. The VUV light source can be a barrier or a corona discharge.

A DBD or surface discharge can have a (small) influence on gas flows. This can be used to improve the flow around an airplane wing, for flame ignition, or for cooling of electrical components. The main advantage of such flow control over conventional methods is that no moving parts are needed and that the size of the device can be kept very small [187, 188].

Occasionally, specific barrier configurations are developed for fundamental investigations. A good example is the single filament electrode geometry developed by Wagner and Kozlov for their cross-correlation spectroscopy [189, 190]. Two

Table 1.2 Barrier discharge applications.

| Discharge type | Application | References |
|----------------------------------|-----------------------------------|----------------|
| Ozone generator | Gas and water cleaning | [184] |
| Surface barrier | Control aerodynamics | [193, 194] |
| Surface barrier | Textile modifications | [16, 116, 156] |
| Atmospheric pressure plasma jet | Microbial decontamination | [163] |
| Plasma needle | Sterilization/wound healing | [160, 195] |
| Excimer lamps | Bacteria removal/ozone generation | [11, 12] |
| Corona with barrier | Phenol/dye removal from water | [7, 196, 197] |
| Microdischarges | Plasma display panels | [18, 159] |
| (Packed bed) barrier | Soot removal diesel engines | [198] |
| Barrier glow discharge | Thin-film deposition solar cells | [17, 19] |
| Barrier with packed bed catalyst | Chemical conversions | [13–15] |

spherical electrodes are used with a gap distance of 1 mm, and one or both are covered with a glass layer. The single filament that develops where the electrodes are closest has such a stable position that the spectra can be recorded by accumulating photons from many pulses. Liu *et al.* have developed a barrier discharge configuration inside a cavity [191]. This enables detection of HO₂ and OH radicals with high sensitivity with the cavity ring down method [192]. Such diagnostics are very important for the development of good models of the chemical activity of the discharge.

A huge amount of literature is available on what can be done with barrier discharges. Only a few examples are mentioned in Table 1.2; in the references given, much more information can be found. At the moment of writing, fast-rising topics are the surface barrier discharges and the plasma jets.

1.5

Gliding Arcs

Arc discharges are thermal discharges and are not considered in this chapter. However, gliding arcs have properties of both thermal and nonthermal plasma conditions. They are highly reactive and often have a high selectivity for chemical processes. The main reason why it is used is because it can provide a plasma with useful properties both from thermal plasmas (large electron densities, currents, and power) and nonthermal plasmas (low gas temperature).

A gliding arc is usually generated between two diverging electrodes typical in a gas flow. The discharge ignites at the shortest distance between the electrodes (few millimeters). Typical breakdown voltages are a few kilovolts. The formation of a hot quasi-thermal plasma corresponds with a decrease in voltage and strong increase in current. Owing to the gas flow (or in absence of the gas flow due

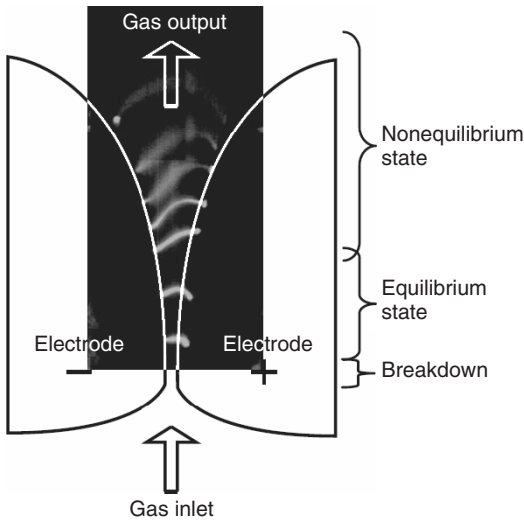


Figure 1.10 Nice example of the superposition of several short exposures of the different stages of a gliding arc discharge. The extension of the discharge channel is clearly visible in the nonthermal stage (upper part). (Source: Taken with permission from Fridman [29].)

to thermal buoyancy) the discharge moves upward and the length of the plasma column increases (see Figure 1.10). This increasing length causes an increase of the heat losses in the column, which exceeds the input energy of the power supply. The quasi-thermal plasma converts into a nonthermal plasma corresponding with a decrease in current and increase in voltage due to the increasing resistivity of the plasma. Eventually, the plasma extinguishes as the power supply cannot maintain such a long plasma column. At this point the recombination of the plasma starts and a reignition of the discharge occurs at the minimum distance between the electrodes. This causes the self-pulsing nature of the gliding arc discharges, which is always clearly visible in current–voltage waveforms and typically occurs on 10 ms timescales.

The exact plasma properties strongly depend on the input power, which can range from about 100 W up to the order of 40 kW. The above description assumes that the transition of a thermal to a nonthermal plasma occurs, although for low powers (and thus low currents) and low flow fields, the gliding arc is nonthermal during its entire lifetime. For the above power range, the gas temperature can range from 2500 up to 10 000 K in the initial “quasi-thermal” state of the plasma. For higher powers, the plasma cools down during the quasi-thermal to nonthermal transition to gas temperatures of 1000–2000 K or even lower, while the electron temperature remains in the order of 1 eV. Note that the largest part of the power is consumed in the nonequilibrium stage of the discharge. Measurements and estimates of the electron density indicate 10^{17} – 10^{18} m^{-3} [199]. The chemical efficiency of these discharges is due to the two phases. In the thermal phase, the molecules introduced

in the discharge are strongly dissociated. The fast transition from a thermal to nonthermal discharge allows a fast recombination of the dissociation products to molecules, which are required for the application. As the flow is rather large, it allows large throughputs with residence times of the reactants in the order of milliseconds. This is the reason why these discharges are typically the workhorses of plasma chemists. Gliding arc discharge has been studied for combustion [200], gas cleaning [200], production of syngas [200], and water treatment [201, 202]. Gliding arcs can also be magnetically stabilized [203]. More details about the physics of gliding discharges can be found in the review papers by Fridman *et al.* [200].

1.6

Concluding Remarks

As in any review of limited length, this work is not complete. We have attempted to include an overview of (recent) work on nonthermal plasmas but realize that it is far from complete. We also had to limit ourselves to the most used nonthermal plasma types. Therefore we have not discussed some recent developments such as plasma jets and plasma bullets in detail. Furthermore, because we have focused on atmospheric pressure plasmas, we have said nothing about microwave-driven plasmas and other nonthermal plasmas that are primarily used at lower pressures.

Some parts of this book deal also with discharges in and in contact with liquids. The main types of discharges are, however, identical to ordinary gas discharges except for some peculiar properties of the so-called direct streamer discharges in liquids [204].

References

1. van Heesch, E.J.M., Winands, G.J.J., and Pemen, A.J.M. (2008) Evaluation of pulsed streamer corona experiments to determine the O* radical yield. *J. Phys. D: Appl. Phys.*, **41** (23), 234015.
2. Heil, B.G., Czarnetzki, U., Brinkmann, R.P., and Mussenbrock, T. (2008) On the possibility of making a geometrically symmetric RF-CCP discharge electrically asymmetric. *J. Phys. D: Appl. Phys.*, **41**, 165202, DOI: 10.1088/0022-3727/41/16/165202.
3. Ebert, U., Nijdam, S., Li, C., Luque, A., Briels, T., and van Veldhuizen, E. (2010) Review of recent results on streamer discharges and discussion of their relevance for sprites and lightning. *J. Geophys. Res.: Space Phys.*, **115**, A00E43.
4. van Veldhuizen, E.M. (2000) *Electrical Discharges for Environmental Purposes: Fundamentals and Applications*, Nova Science Publishers, New York.
5. Winands, G.J.J., Liu, Z., Pemen, A.J.M., van Heesch, E.J.M., and Yan, K. (2008) Analysis of streamer properties in air as function of pulse and reactor parameters by iccd photography. *J. Phys. D: Appl. Phys.*, **41**, 234001.
6. Grabowski, L., van Veldhuizen, E., Pemen, A., and Rutgers, W. (2006) Corona above water reactor for systematic study of aqueous phenol degradation. *Plasma Chem. Plasma Process.*, **26**, 3–17, doi: 10.1007/s11090-005-8721-8
7. Malik, M.A. (2010) Water purification by plasmas: which reactors are most energy efficient? *Plasma Chem. Plasma Process.*, **30**, 21–31.

8. Braun, D., Kuechler, U., and Pietsch, G. (1991) Microdischarges in air-fed ozonizers. *J. Phys. D: Appl. Phys.*, **24**, 564–572.
9. Eliasson, B., Hirth, M., and Kogelschatz, U. (1986) Ozone synthesis from oxygen in dielectric barrier discharges. *J. Phys. D: Appl. Phys.*, **20**, 1421–1437.
10. Šimor, M., Ráhel, J., Vojtek, P., Cernák, M., and Brablec, A. (2002) Atmospheric-pressure diffuse coplanar surface discharge for surface treatments. *Appl. Phys. Lett.*, **81**, 2716–2718.
11. Salvermoser, M., Murnick, D., and Kogelschatz, U. (2008) Influence of water vapor on photochemical ozone generation with efficient 172 nm xenon excimer lamps. *Ozone Sci. Eng.*, **30**, 228–237.
12. Erofeev, M.V., Schitz, D.V., Skakun, V.S., Sosnin, E.A., and Tarasenko, V.F. (2010) Compact dielectric barrier discharge excilamps. *Phys. Scr.*, **82**, 045403.
13. Horvath, G., Mason, N.J., Polachova, L., Zahoran, M., Moravsky, L., and Matejcik, S. (2010) Packed bed DBD discharge experiments in admixtures of N₂ and CH₄. *Plasma Chem. Plasma Process.*, **30**, 565–577.
14. Mok, Y.S., Kang, H.C., Lee, H.J., Koh, D.J., and Shin, D.N. (2010) Effect of nonthermal plasma on the methanation of carbon monoxide over nickel catalyst. *Plasma Chem. Plasma Process.*, **30**, 437–447.
15. Huang, L., Xing-wang, Z., Chen, L., and Le-cheng, L. (2011) Direct oxidation of methane to methanol over cu-based catalyst in an ac dielectric barrier discharge. *Plasma Chem. Plasma Process.*, **31**, 67–77, DOI: 10.1007/s11090-010-9272-1.
16. Cernak, M., Cernakova, L., Hudec, I., Kovacic, D., and Zahoranov, A. (2009) Diffuse coplanar surface barrier discharge and its applications for in-line processing of low-added-value materials. *Eur. Phys. J. Appl. Phys.*, **47**, 22806.
17. Starostin, S., Premkumar, P.A., van Veldhuizen, M.C.E., de Vries, H., Paffen, R., and van de Sanden, M. (2009) On the formation mechanisms of the diffuse atmospheric pressure dielectric barrier discharge in cvd processes of thin silica-like films. *Plasma Sources Sci. Technol.*, **18**, 045021.
18. Klages, C.P., Hinze, A., Lachmann, K., Berger, C., Borris, J., Eichler, M., von Hausen, M., Zänker, A., and Thomas, M. (2007) Surface technology with cold microplasmas. *Plasma Processes Polym.*, **4**, 208–218.
19. Sarra-Bournet, C., Gherardi, N., Glénat, H., Laroche, G., and Massines, F. (2010) Effect of C₂H₄/N₂ ratio in an atmospheric pressure dielectric barrier discharge on the plasma deposition of hydrogenated amorphous carbon-nitride films (a-C:N:H). *Plasma Chem. Plasma Process.*, **30**, 213–239.
20. Caruana, D. (2010) Plasmas for aerodynamic control. *Plasma Phys. Control. Fusion*, **52**, 124045.
21. Starikovskii, A., Nikipelov, A., Nudnova, M., and Roupasov, D. (2009) Sdbd plasma actuator with nanosecond pulse-periodic discharge. *Plasma Sources Sci. Technol.*, **18**, 034015.
22. Unfer, T. and Boeuf, J. (2009) Modelling of a nanosecond surface discharge actuator. *J. Phys. D: Appl. Phys.*, **42**, 194017.
23. Foest, R., Kindel, E., Lange, H., Ohl, A., Stieber, M., and Weltmann, K.D. (2007) Rf capillary jet – a tool for localized surface treatment. *Contrib. Plasma Phys.*, **47**, 119–128.
24. Laroussi, M. and Lu, X. (2005) Room-temperature atmospheric pressure plasma plume for biomedical applications. *Appl. Phys. Lett.*, **87**, 113902.
25. Pai, D.Z., Stancu, G.D., Lacoste, D.A., and Laux, C.O. (2009) Nanosecond repetitively pulsed discharges in air at atmospheric pressure—the glow regime. *Plasma Sources Sci. Technol.*, **18** (4), 045030.
26. Baars-Hibbe, L., Sichler, P., Schrader, C., Lucas, N., Gericke, K.H., and Büttgenbach, S. (2005) High frequency glow discharges at atmospheric pressure with micro-structured electrode

- arrays. *J. Phys. D: Appl. Phys.*, **38**, 510–517.
27. Becker, K., Schoenbach, K., and Eden, J. (2006) Microplasmas and applications. *J. Phys. D: Appl. Phys.*, **39**, R55–R70.
 28. Hrycak, B., Jasinski, M., and Mizeraczyk, J. (2010) Spectroscopic investigations of microwave microplasmas in various gases at atmospheric pressure. *Eur. Phys. J. D*, **60**, 609–619.
 29. Fridman, A. (2008) *Plasma Chemistry*, Cambridge University Press.
 30. Bruggeman, P., Walsh, J.L., Schram, D.C., Leys, C., and Kong, M.G. (2009) Time dependent optical emission spectroscopy of sub-microsecond pulsed plasmas in air with water cathode. *Plasma Sources Sci. Technol.*, **18** (4), 045023.
 31. Li, C., Brok, W.J.M., Ebert, U., and van der Mullen, J.J.A.M. (2007) Deviations from the local field approximation in negative streamer heads. *J. Appl. Phys.*, **101** (12), 123305.
 32. Li, C., Ebert, U., and Hundsdorfer, W. (2010) Spatially hybrid computations for streamer discharges with generic features of pulled fronts: I. planar fronts. *J. Comput. Phys.*, **229** (1), 200–220.
 33. Kossyi, I.A., Kostinsky, A.Y., Matveyev, A.A., and Silakov, V.P. (1992) Kinetic scheme of the non-equilibrium discharge in nitrogen-oxygen mixtures. *Plasma Sources Sci. Technol.*, **1**, 207.
 34. Morrow, R. and Lowke, J.J. (1997) Streamer propagation in air. *J. Phys. D: Appl. Phys.*, **30**, 614.
 35. Liu, N. and Pasko, V.P. (2004) Effects of photoionization on propagation and branching of positive and negative streamers in sprites. *J. Geophys. Res.*, **109**, 1.
 36. Dujko, S., Ebert, U., White, R., and Petrovic, Z. (2011) Boltzmann equation analysis of electron transport in a N₂-O₂ streamer discharge. *Jap. J. Appl. Phys.* **50**, 08JC01, DOI: 10.1143/JJAP.50.08JC01.
 37. Nikonov, V., Bartnikas, R., and Wertheimer, M. (2001) Surface charge and photoionization effects in short air gaps undergoing discharges at atmospheric pressure. *J. Phys. D: Appl. Phys.*, **34**, 2979–2986.
 38. Auday, G., Guillot, P., and Galy, J. (2000) Secondary emission of di-electrics used in plasma display panels. *J. Appl. Phys.*, **88**, 4871–4874.
 39. Josepson, R., Laan, M., Aarik, J., and Kasikov, A. (2008) Photoinduced field-assisted electron emission from dielectric-coated electrodes into gases. *J. Phys. D: Appl. Phys.*, **42**, 135209.
 40. Fridman, A., Chirokov, A., and Gutsol, A. (2005) Non-thermal atmospheric pressure discharges. *J. Phys. D: Appl. Phys.*, **38**, R1.
 41. Chang, J., Lawless, P., and Yamamoto, T. (1991) Corona discharge processes. *IEEE Trans. Plasma Sci.*, **19** (6), 1152–1166.
 42. Ono, R. and Oda, T. (2007) Ozone production process in pulsed positive dielectric barrier discharge. *J. Phys. D: Appl. Phys.*, **40** (1), 176.
 43. Kim, H. (2004) Nonthermal plasma processing for air-pollution control: a historical review, current issues, and future prospects. *Plasma Process. Polym.*, **1** (2), 91–110.
 44. Namihira, T., Wang, D., Katsuki, S., Hackam, R., and Akiyama, H. (2003) Propagation velocity of pulsed streamer discharges in atmospheric air. *IEEE Trans. Plasma Sci.*, **31** (5), 1091.
 45. Penetrante, B.M. (1993) *Non-Thermal Plasma Techniques for Pollution Control*, NATO ASI Series, Vol. G34, Springer-Verlag, pp. 65–89.
 46. Urashima, K., Chang, J.S., Park, J.Y., Lee, D.C., Chakrabarti, A., and Ito, T. (1998) Reduction of nox from natural gas combustion flue gases by corona discharge radical injection techniques [thermal power plant emissions control]. *IEEE Trans. Ind. Appl.*, **34** (5), 934–939.
 47. Penetrante, B.M., Hsiao, M.C., Merritt, B.T., Vogtlin, G.E., Wallman, P.H., Neiger, M., Wolf, O., Hammer, T., and Broer, S. (1996) Pulsed corona and dielectric-barrier discharge processing of NO in N₂. *Appl. Phys. Lett.*, **68** (26), 3719–3721.

48. Itikawa, Y. and Mason, N. (2005) Cross sections for electron collisions with water molecules. *J. Phys. Chem. Ref. Data*, **34** (1), 1–22.
49. Bruggeman, P. and Schram, D.C. (2010) On OH production in water containing atmospheric pressure plasmas. *Plasma Sources Sci. Technol.*, **19** (4), 045025.
50. Rehbein, N. and Cooray, V. (2001) Nox production in spark and corona discharges. *J. Electrostat.*, **51–52**, 333–339.
51. Eliasson, B. and Kogelschatz, U. (1991) Modelling and applications of silent discharge plasmas. *IEEE Trans. Plasma Sci.*, **19**, 309–323.
52. Aleksandrov, N.L. and Bazelyan, E.M. (1999) Ionization processes in spark discharge plasmas. *Plasma Sources Sci. Technol.*, **8**, 285.
53. Laux, C., Spence, T., Kruger, C., and Zare, R. (2003) Optical diagnostics of atmospheric pressure air plasmas. *Plasma Sources Sci. Technol.*, **12** (2), 125–138.
54. Kozlov, K.V., Wagner, H.E., Brandenburg, R., and Michel, P. (2001) Spatio-temporally resolved spectroscopic diagnostics of the barrier discharge in air at atmospheric pressure. *J. Phys. D: Appl. Phys.*, **34** (21), 3164.
55. Liu, N., Pasko, V.P., Burkhardt, D.H., Frey, H.U., Mende, S.B., Su, H.T., Chen, A.B., Hsu, R.R., Lee, L.C., Fukunishi, H. *et al.* (2006) Comparison of results from sprite streamer modeling with spectrophotometric measurements by ISUAL instrument on FORMOSAT-2 satellite. *Geophys. Res. Lett.*, **33**, 01101.
56. Bruggeman, P., Iza, F., Guns, P., Lauwers, D., Kong, M.G., Gonzalvo, Y.A., Leys, C., and Schram, D.C. (2010) Electronic quenching of OH(A) by water in atmospheric pressure plasmas and its influence on the gas temperature determination by OH(A – X) emission. *Plasma Sources Sci. Technol.*, **19** (1), 015016.
57. Niemi, K., Gathen, V., and Döbele, H. (2005) Absolute atomic oxygen density measurements by two-photon absorption laser-induced fluorescence spectroscopy in an RF-excited atmospheric pressure plasma jet. *Plasma Sources Sci. Technol.*, **14**, 375.
58. Stancu, G.D., Kaddouri, F., Lacoste, D.A., and Laux, C.O. (2010) Atmospheric pressure plasma diagnostics by OES, CRDS and TALIF. *J. Phys. D: Appl. Phys.*, **43** (12), 124002.
59. Muraoka, K. and Kono, A. (2011) Laser Thomson scattering for low-temperature plasmas. *J. Phys. D: Appl. Phys.*, **44** (4), 043001.
60. Palomares, J.M., Iordanova, E.I., Gamero, A., Sola, A., and van der Mullen, J.J.A.M. (2010) Atmospheric microwave-induced plasmas in Ar/H₂ mixtures studied with a combination of passive and active spectroscopic methods. *J. Phys. D: Appl. Phys.*, **43** (39), 395202.
61. Stoffels, E., Gonzalvo, Y.A., Whitmore, T.D., Seymour, D.L., and Rees, J.A. (2007) Mass spectrometric detection of short-living radicals produced by a plasma needle. *Plasma Sources Sci. Technol.*, **16** (3), 549.
62. Bruggeman, P., Iza, F., Lauwers, D., and Gonzalvo, Y.A. (2010) Mass spectrometry study of positive and negative ions in a capacitively coupled atmospheric pressure RF excited glow discharge in He-water mixtures. *J. Phys. D: Appl. Phys.*, **43** (1), 012003.
63. Clements, J.S., Mizuno, A., Finney, W.C., and Davis, R.H. (1989) Combined removal of SO₂, NO_x, and fly ash from simulated flue gas using pulsed streamer corona. *IEEE Trans. Ind. Appl.*, **25** (1), 62–69.
64. Winands, G.J.J., Yan, K., Pemen, A.J.M., Nair, S.A., Liu, Z., and van Heesch, E.J.M. (2006) An industrial streamer corona plasma system for gas cleaning. *IEEE Trans. Plasma Sci.*, **34** (5, Part 4), 2426–2433.
65. Kogelschatz, U. (2004) Atmospheric-pressure plasma technology. *Plasma Phys. Control. Fusion*, **46** (12B), B63.
66. Eichwald, O., Ducasse, O., Dubois, D., Abahazem, A., Merbahi, N., Benhenni, M., and Yousfi, M. (2008) Experimental analysis and modelling of positive

- streamer in air: towards an estimation of O and N radical production. *J. Phys. D: Appl. Phys.*, **41** (23), 234002.
67. Morrow, R. (1997) The theory of positive glow corona. *J. Phys. D: Appl. Phys.*, **30** (22), 3099.
 68. Shang, K. and Wu, Y. (2010) Effect of electrode configuration and corona polarity on NO removal by pulse corona plasma. Power and Energy Engineering Conference (APPEEC), 2010 Asia-Pacific, pp. 1–4.
 69. Yan, K., van Hoesch, E.J.M., Pemen, A.J.M., and Huijbrechts, P.A.H.J. (2001) From chemical kinetics to streamer corona reactor and voltage pulse generator. *Plasma Chem. Plasma Process.*, **21**, 107–137.
 70. Ratushnaya, V., Luque, A., and Ebert, U. (2012) Electrodynamic characterization of long positive streamers in air. *J. Phys. D: Appl. Phys.*, in preparation.
 71. Ebert, U., Brau, F., Derks, G., Hundsdorfer, W., Kao, C.Y., Li, C., Luque, A., Meulenbroek, B., Nijdam, S., Ratushnaya, V., Schäfer, L., and Tanveer, S. (2011) Multiple scales in streamer discharges, with an emphasis on moving boundary approximations. *Nonlinearity*, **24**, C1.
 72. Babich, L.P. (2003) *High-Energy Phenomena in Electric Discharges in Dense Gases*, Futurepast Inc, Arlington, VA.
 73. Moss, G.D., Pasko, V.P., Liu, N., and Veronis, G. (2006) Monte carlo model for analysis of thermal runaway electrons in streamer tips in transient luminous events and streamer zones of lightning leaders. *J. Geophys. Res.*, **111** (A2), A02307.
 74. Li, C., Ebert, U., and Hundsdorfer, W. (2009) 3D hybrid computations for streamer discharges and production of run-away electrons. *J. Phys. D: Appl. Phys.*, **42** (202003), 202–203.
 75. Chanrion, O. and Neubert, T. (2010) Production of runaway electrons by negative streamer discharges. *J. Geophys. Res.*, **115**, A00E32.
 76. Nguyen, C.V., van Deursen, A.P.J., and Ebert, U. (2008) Multiple X-ray bursts from long discharges in air. *J. Phys. D: Appl. Phys.*, **41**, 234012.
 77. Briels, T.M.P., Kos, J., van Veldhuizen, E.M., and Ebert, U. (2006) Circuit dependence of the diameter of pulsed positive streamers in air. *J. Phys. D: Appl. Phys.*, **39**, 5201.
 78. Briels, T.M.P., Kos, J., Winands, G.J.J., van Veldhuizen, E.M., and Ebert, U. (2008) Positive and negative streamers in ambient air: measuring diameter, velocity and dissipated energy. *J. Phys. D: Appl. Phys.*, **41**, 234004.
 79. Naidis, G.V. (2009) Positive and negative streamers in air: velocity-diameter relation. *Phys. Rev. E*, **79** (5), 057401.
 80. Luque, A. and Ebert, U. (2010) Sprites in varying air density: charge conservation, glowing negative trails and changing velocity. *Geophys. Res. Lett.*, **31**, L06806.
 81. Luque, A., Ratushnaya, V., and Ebert, U. (2008) Positive and negative streamers in ambient air: modeling evolution and velocities. *J. Phys. D: Appl. Phys.*, **41**, 234005.
 82. Luque, A. and Ebert, U. (2012) Density models for streamer discharges: beyond cylindrical symmetry and homogeneous media. *J. Comput. Phys.*, **231**, 904–918, DOI: 10.1016/j.jcp.2011.04.019.
 83. Li, C., Ebert, U., and Hundsdorfer, W. (2012) Spatially hybrid computations for streamer discharges: II. fully 3D simulations. *J. Comput. Phys.*, **231**, 1020–1050, DOI: 10.1016/j.jcp.2011.07.023.
 84. Mathew, D., Bastiaens, H.M.J., Boller, K.J., and Peters, P.J.M. (2007) Effect of preionization, fluorine concentration, and current density on the discharge uniformity in F2 excimer laser gas mixtures. *J. Appl. Phys.*, **102** (3), 033305.
 85. Meek, J.M. (1940) A theory of spark discharge. *Phys. Rev.*, **57** (8), 722–728.
 86. Raether, H. (1939) Die entwicklung der elektronenlawine in den funkenkanal. *Z. Phys. A: Hadrons Nuclei*, **112** (7), 464–489.
 87. Montijn, C. and Ebert, U. (2006) Diffusion correction to the Raether and Meek criterion for the avalanche-to-streamer transition. *J. Phys. D: Appl. Phys.*, **39**, 2979.

88. Pancheshnyi, S. (2005) Role of electronegative gas admixtures in streamer start, propagation and branching phenomena. *Plasma Sources Sci. Technol.*, **14**, 645.
89. Wormeester, G., Pancheshnyi, S., Luque, A., Nijdam, S., and Ebert, U. (2010) Probing photo-ionization: simulations of positive streamers in varying N₂:O₂-mixtures. *J. Phys. D: Appl. Phys.*, **43**, 505201, DOI: 10.1088/0022-3727/43/50/505201.
90. Luque, A., Ebert, U., Montijn, C., and Hundsdorfer, W. (2007) Photoionisation in negative streamers: fast computations and two propagation modes. *Appl. Phys. Lett.*, **90**, 081501, DOI: 10.1063/1.2435934.
91. Briels, T.M.P., van Veldhuizen, E.M., and Ebert, U. (2008) Positive streamers in air and nitrogen of varying density: experiments on similarity laws. *J. Phys. D: Appl. Phys.*, **41**, 234008.
92. Briels, T.M.P., van Veldhuizen, E.M., and Ebert, U. (2008) Positive streamers in ambient air and a N₂:O₂-mixture (99.8: 0.2). *IEEE Trans. Plasma Sci.*, **36**, 906–907.
93. Nijdam, S., Miermans, K., van Veldhuizen, E., and Ebert, U. (2011) A peculiar streamer morphology created by a complex voltage pulse. *IEEE Trans. Plasma Sci.*, **39**, 2216–2217, DOI: 10.1109/TPS.2011.2158661.
94. Briels, T.M.P., van Veldhuizen, E.M., and Ebert, U. (2005) Branching of positive discharge streamers in air at varying pressures. *IEEE Trans. Plasma Sci.*, **33**, 264.
95. Ebert, U., Montijn, C., Briels, T.M.P., Hundsdorfer, W., Meulenbroek, B., Rocco, A., and van Veldhuizen, E.M. (2006) The multiscale nature of streamers. *Plasma Sources Sci. Technol.*, **15**, S118.
96. Marode, E. (1975) The mechanism of spark breakdown in air at atmospheric pressure between a positive point and a plane. I. experimental: nature of the streamer track. *J. Appl. Phys.*, **46** (5), 2005–2015.
97. Sigmond, R.S. (1984) The residual streamer channel: return strokes and secondary streamers. *J. Appl. Phys.*, **56** (5), 1355–1370.
98. Ono, R. and Oda, T. (2003) Formation and structure of primary and secondary streamers in positive pulsed corona discharge-effect of oxygen concentration and applied voltage. *J. Phys. D: Appl. Phys.*, **36** (16), 1952–1958.
99. Liu, N. (2010) Model of sprite luminous trail caused by increasing streamer current. *Geophys. Res. Lett.*, **37**, L04102.
100. Nijdam, S., Moerman, J.S., Briels, T.M.P., van Veldhuizen, E.M., and Ebert, U. (2008) Stereo-photography of streamers in air. *Appl. Phys. Lett.*, **92**, 101502.
101. Nijdam, S., Geurts, C.G.C., van Veldhuizen, E.M., and Ebert, U. (2009) Reconnection and merging of positive streamers in air. *J. Phys. D: Appl. Phys.*, **42** (4), 045201.
102. Arrayás, M., Ebert, U., and Hundsdorfer, W. (2002) Spontaneous branching of anode-directed streamers between planar electrodes. *Phys. Rev. Lett.*, **88** (17), 174502.
103. Montijn, C., Ebert, U., and Hundsdorfer, W. (2006) Numerical convergence of the branching time of negative streamers. *Phys. Rev. E*, **73** (6), 65401.
104. Luque, A. and Ebert, U. (2011) Electron density fluctuations accelerate the branching of streamer discharges in air. *Phys. Rev. E*, **84**, 046411, DOI: 10.1103/PhysRevE.84.046411.
105. Loeb, L.B. and Meek, J.M. (1940) The mechanism of spark discharge in air at atmospheric pressure. I. *J. Appl. Phys.*, **11** (6), 438–447.
106. Nijdam, S., van de Wetering, F.M.J.H., Blanc, R., van Veldhuizen, E.M., and Ebert, U. (2010) Probing photo-ionization: experiments on positive streamers in pure gases and mixtures. *J. Phys. D: Appl. Phys.*, **43**, 145204.
107. Wormeester, G., Nijdam, S., and Ebert, U. (2011) Feather-like structures in positive streamers. *Jap. J. Appl. Phys.*, **50**, 08JA01, DOI: 10.1143/JJAP.50.08JA01.

108. van Veldhuizen, E.M. and Rutgers, W.R. (2002) Pulsed positive corona streamer propagation and branching. *J. Phys. D: Appl. Phys.*, **35**, 2169.
109. Babaeva, N.Y. and Kushner, M.J. (2008) Streamer branching: the role of inhomogeneities and bubbles. *IEEE Trans. Plasma Sci.*, **36** (4), 892–893.
110. Niemeyer, L., Pietronero, L., and Wiesmann, H.J. (1984) Fractal dimension of dielectric breakdown. *Phys. Rev. Lett.*, **52**, 1033.
111. Pasko, V.P., Inan, U.S., and Bell, T.F. (1998) Spatial structure of sprites. *Geophys. Res. Lett.*, **25**, 2123–2126.
112. Akyuz, M., Larsson, A., Cooray, V., and Strandberg, G. (2003) 3D simulations of streamer branching in air. *J. Electrostat.*, **59**, 115.
113. Raizer, Y.P. (1991) *Gas Discharge Physics*, Springer-Verlag, Berlin.
114. Šijacic, D.D. and Ebert, U. (2002) Transition from townsend to glow discharge: subcritical, mixed, or supercritical characteristics. *Phys. Rev. E*, **66** (6), 066410.
115. von Engel, A., Seeliger, R., and Steinbeck, M. (1933) Über die Glimmentladung bei hohen Drucken. *Z. Phys.*, **85**, 144.
116. Massines, F. and Gouda, G. (1998) A comparison of polypropylene-surface treatment by filamentary, homogeneous and glow discharges in helium at atmospheric pressure. *J. Phys. D: Appl. Phys.*, **31**, 3411–3420.
117. Kunhardt, E. (2000) Generation of large – volume, atmospheric – pressure, nonequilibrium plasmas. *IEEE Trans. Plasma Sci.*, **28** (1), 189–200.
118. Barinov, Y., Kaplan, V., Rozhdestvenskii, V., and Shkolnik, S. (1998) Determination of the electron density in a discharge with nonmetallic liquid electrodes in atmospheric-pressure air from the absorption of microwave probe radiation. *Tech. Phys. Lett.*, **24** (12), 929–931.
119. Lu, X.P. and Laroussi, M. (2008) Electron density and temperature measurement of an atmospheric pressure plasma by millimeter wave interferometer. *Appl. Phys. Lett.*, **92** (5), 051501.
120. Bruggeman, P., Liu, J., Degroote, J., Kong, M.G., Vierendeels, J., and Leys, C. (2008) Dc excited glow discharges in atmospheric pressure air in pin-to-water electrode systems. *J. Phys. D: Appl. Phys.*, **41** (21), 215201.
121. Staack, D., Farouk, B., Gutsol, A.F., and Fridman, A. (2007) Spatially resolved temperature measurements of atmospheric-pressure normal glow microplasmas in air. *IEEE Trans. Plasma Sci.*, **35** (5, Part 2), 1448–1455.
122. Iza, F., Lee, J.K., and Kong, M.G. (2007) Electron kinetics in radio-frequency atmospheric-pressure microplasmas. *Phys. Rev. Lett.*, **99** (7), 075004.
123. Aldea, E., Peeters, P., de Vries, H., and van de Sanden, M. (2005) Atmospheric glow stabilization. do we need pre-ionization? *Surf. Coat. Technol.*, **200**, 46–50.
124. Laroussi, M., Alexeff, I., Richardson, J., and Dyer, F. (2002) The resistive barrier discharge. *IEEE Trans. Plasma Sci.*, **30** (1, Part 1), 158–159.
125. Andre, P., Barinov, Y., Faure, G., Kaplan, V., Lefort, A., Shkol'nik, S., and Vacher, D. (2001) Experimental study of discharge with liquid non-metallic (tap-water) electrodes in air at atmospheric pressure. *J. Phys. D: Appl. Phys.*, **34** (24), 3456–3465.
126. Lu, X. and Laroussi, M. (2005) Atmospheric pressure glow discharge in air using a water electrode. *IEEE Trans. Plasma Sci.*, **33** (2, Part 1), 272–273.
127. Bruggeman, P., Ribezl, E., Maslani, A., Degroote, J., Malesevic, A., Rego, R., Vierendeels, J., and Leys, C. (2008) Characteristics of atmospheric pressure air discharges with a liquid cathode and a metal anode. *Plasma Sources Sci. Technol.*, **17** (2), 025012.
128. Gherardi, N. and Massines, F. (2001) Mechanisms controlling the transition from glow silent discharge to streamer discharge in nitrogen. *IEEE Trans. Plasma Sci.*, **29** (3), 536–544.
129. Massines, F., Rabehi, A., Decomps, P., Gadri, R., Segur, P., and Mayoux, C. (1998) Experimental and theoretical study of a glow discharge at atmospheric pressure controlled by

- dielectric barrier. *J. Appl. Phys.*, **83** (6), 2950–2957.
130. Gherardi, N., Gouda, G., Gat, E., Ricard, A., and Massines, F. (2000) Transition from glow silent discharge to micro-discharges in nitrogen gas. *Plasma Sources Sci. Technol.*, **9**, 340.
 131. Raizer, Y.P., Ebert, U., and Šijacic, D. (2004) Dependence of the transition from Townsend to glow discharge on secondary emission. *Phys. Rev. E*, **70** (1), 17401.
 132. Šijacic, D.D., Ebert, U., and Rafatov, I. (2004) Period doubling cascade in glow discharges: local versus global differential conductivity. *Phys. Rev. E*, **70** (5), 056220.
 133. Šijacic, D.D., Ebert, U., and Rafatov, I. (2005) Oscillations in dc driven barrier discharges: numerical solutions, stability analysis, and phase diagram. *Phys. Rev. E*, **71** (6), 066402.
 134. Rafatov, I.R., Šijacic, D.D., and Ebert, U. (2007) Spatiotemporal patterns in a dc semiconductor-gas-discharge system: stability analysis and full numerical solutions. *Phys. Rev. E*, **76** (3), 036206.
 135. Raizer, Y.P., Gurevich, E.L., and Mokrov, M.S. (2006) Self-sustained oscillations in a low-current discharge with a semiconductor serving as a cathode and ballast resistor: II. Theory. *Tech. Phys.*, **51** (2), 185–197.
 136. Shi, J., Deng, X., Hall, R., Punnett, J., and Kong, M. (2003) Three modes in a radio frequency atmospheric pressure glow discharge. *J. Appl. Phys.*, **94** (10), 6303–6310.
 137. Shi, J. and Kong, M. (2005) Mechanisms of the alpha and gamma modes in radio-frequency atmospheric glow discharges. *J. Appl. Phys.*, **97** (2), 023306.
 138. Goossens, O., Callebaut, T., Akishev, Y., Napartovich, A., Trushkin, N., and Leys, C. (2002) The DC glow discharge at atmospheric pressure. *IEEE Trans. Plasma Sci.*, **30** (1, Part 1), 176–177.
 139. Akishev, Y., Goossens, O., Callebaut, T., Leys, C., Napartovich, A., and Trushkin, N. (2001) The influence of electrode geometry and gas flow on corona-to-glow and glow-to-spark threshold currents in air. *J. Phys. D: Appl. Phys.*, **34** (18), 2875–2882.
 140. Machala, Z., Janda, M., Hensel, K., Jedlovsky, I., Lestinska, L., Foltin, V., Martisovits, V., and Morvova, M. (2007) Emission spectroscopy of atmospheric pressure plasmas for bio-medical and environmental applications. *J. Mol. Spectrosc.*, **243** (2), 194–201.
 141. Schulz-von der Gathen, V., Schaper, L., Knake, N., Reuter, S., Niemi, K., Gans, T., and Winter, J. (2008) Spatially resolved diagnostics on a microscale atmospheric pressure plasma jet. *J. Phys. D: Appl. Phys.*, **41** (19), 194004.
 142. Waskoenig, J., Niemi, K., Knake, N., Graham, L.M., Reuter, S., Schulz-von der Gathen, V., and Gans, T. (2010) Atomic oxygen formation in a radio-frequency driven micro-atmospheric pressure plasma jet. *Plasma Sources Sci. Technol.*, **19** (4), 045018.
 143. Niemi, K., Reuter, S., Graham, L.M., Waskoenig, J., and Gans, T. (2009) Diagnostic based modeling for determining absolute atomic oxygen densities in atmospheric pressure helium-oxygen plasmas. *Appl. Phys. Lett.*, **95** (15), 151504.
 144. Liu, D.X., Rong, M.Z., Wang, X.H., Iza, F., Kong, M.G., and Bruggeman, P. (2010) Main species and physicochemical processes in cold atmospheric-pressure He + O-2 plasmas. *Plasma Process. Polym.*, **7** (9–10), 846–865.
 145. Liu, D.X., Bruggeman, P., Iza, F., Rong, M.Z., and Kong, M.G. (2010) Global model of low-temperature atmospheric-pressure He + H₂O plasmas. *Plasma Sources Sci. Technol.*, **19** (2), 025018.
 146. Akishev, Y., Grushin, M., Kochetov, I., Karalnik, V., Napartovich, A., and Trushkin, N. (2005) Negative corona, glow and spark discharges in ambient air and transitions between them. *Plasma Sources Sci. Technol.*, **14** (2), S18–S25.
 147. Korolev, Y.D., Frants, O.B., Landl, N.V., Geyman, V.G., and Matveev, I.B. (2007) Glow-to-spark transitions in a plasma system for ignition and combustion

- control. *IEEE Trans. Plasma Sci.*, **35** (6, Part 1), 1651–1657.
148. Lewis, D. and Woolsey, G. (1981) Spark discharges in iodine vapour. *J. Phys. D: Appl. Phys.*, **14** (8), 1445–1158.
 149. Takaki, K., Kitamura, D., and Fujiwara, T. (2000) Characteristics of a high-current transient glow discharge in dry air. *J. Phys. D: Appl. Phys.*, **33** (11), 1369–1375.
 150. Chalmers, I. and Duffy, H. (1971) Observations of arc-forming stages of spark breakdown using an image intensifier and converter. *J. Phys. D: Appl. Phys.*, **4** (9), 1302–1305.
 151. Bruggeman, P., Guns, P., Degroote, J., Vierendeels, J., and Leys, C. (2008) Influence of the water surface on the glow-to-spark transition in a metal-pin-to-water electrode system. *Plasma Sources Sci. Technol.*, **17** (4), 045014.
 152. Chalmers, I. (1971) Transient glow discharge in nitrogen and dry air. *J. Phys. D: Appl. Phys.*, **4** (8), 1147.
 153. Suleebka, P., Barrault, M., and Craggs, J. (1975) Constriction of a high-pressure glow-discharge in hydrogen. *J. Phys. D: Appl. Phys.*, **8** (18), 2190–2297.
 154. Pai, D.Z., Lacoste, D.A., and Laux, C.O. (2010) Transitions between corona, glow, and spark regimes of nanosecond repetitively pulsed discharges in air at atmospheric pressure. *J. Appl. Phys.*, **107** (9), 093303.
 155. Morshuis, P. (2005) Degradation of solid dielectrics due to internal partial discharge. *IEEE Trans. Dielectrics Electr. Insul.*, **12**, 905–913.
 156. Onsuratoom, S., Rujiravanit, R., Sreethawong, T., Tokura, S., and Chavadej, S. (2010) Silver loading on dbd plasma-modified woven pet surface for antimicrobial property improvement. *Plasma Chem. Plasma Process.*, **30**, 191–206.
 157. Stollenwerk, L. (2010) Interaction of current filaments in a dielectric barrier discharge system. *Plasma Phys. Control. Fusion*, **52**, 124017.
 158. Masuda, S., Akutsu, K., Kuroda, M., Awatsu, Y., and Shibuya, Y. (1988) A ceramic-based ozonizer using high-frequency discharge. *IEEE Trans. Ind. Appl.*, **24**, 223–231.
 159. Hagelaar, G., Klein, M., Snijkers, R., and Kroesen, G. (2001) Energy loss mechanisms in the microdischarges in plasma display panels. *J. Appl. Phys.*, **89**, 2033–2039.
 160. Stoffels, E., Sakiyama, Y., and Graves, D. (2008) Cold atmospheric plasma: charged species and their interactions with cells and tissues. *IEEE Trans. Plasma Sci.*, **36**, 1441–1457.
 161. Stoffels, E., Flikweert, A., Stoffels, W., and Kroesen, G. (2002) Plasma needle: a non-destructive atmospheric plasma source for fine surface treatment of (bio)materials. *Plasma Sources Sci. Technol.*, **11**, 383–388.
 162. Jiang, N., Ji, A., and Cao, Z. (2010) Atmospheric pressure plasma jets beyond ground electrode as charge overflow in a dielectric barrier discharge setup. *J. Appl. Phys.*, **108**, 033302.
 163. Ehlbeck, J., Schnabel, U., Polak, M., Winter, J., von Woedtke, T., Brandenburg, R., von dem Hagen, T., and Weltmann, K.D. (2011) Low temperature atmospheric pressure plasma sources for microbial decontamination (topical review). *J. Phys. D: Appl. Phys.*, **44**, 013002.
 164. Lee, H., Park, G., Seo, Y., Im, Y., Shim, S., and Lee, H. (2011) Modelling of atmospheric pressure plasmas for biomedical applications. *J. Phys. D: Appl. Phys.*, **44**, 053001, DOI: 10.1088/0022-3727/44/5/053001.
 165. Jarrige, J., Laroussi, M., and Karakas, E. (2010) Formation and dynamics of plasma bullets in a non-thermal plasma jet: influence of the high-voltage parameters on the plume characteristics. *Plasma Sources Sci. Technol.*, **19**, 065005.
 166. Dhali, S.K. and Williams, P.F. (1987) Two-dimensional studies of streamers in gases. *J. Appl. Phys.*, **62** (12), 4696–4707.
 167. Gallimberti, I. (1988) Impulse corona simulation for flue gas treatment. *Pure Appl. Chem.*, **60**, 663–674.
 168. Babaeva, N.Y. and Naidis, G.V. (1996) Two-dimensional modelling of positive streamer dynamics in non-uniform

- electric fields in air. *J. Phys. D: Appl. Phys.*, **29**, 2423.
169. Vitello, P.A., Penetrante, B.M., and Bardsley, J.N. (1994) Simulation of negative-streamer dynamics in nitrogen. *Phys. Rev. E*, **49** (6), 5574–5598.
 170. Balcon, N., Aanesland, A., and Boswell, R. (2007) Pulsed rf discharges, glow and filamentary mode at atmospheric pressure in argon. *Plasma Sources Sci. Technol.*, **16** (2), 217.
 171. Dong, L., Qi, Y., Zhao, Z., and Li, Y. (2008) Electron density of an individual microdischarge channel in patterns in a dielectric barrier discharge at atmospheric pressure. *Plasma Sources Sci. Technol.*, **17** (1), 015015.
 172. Zhu, X.M., Pu, Y.K., Balcon, N., and Boswell, R. (2009) Measurement of the electron density in atmospheric-pressure low-temperature argon discharges by line-ratio method of optical emission spectroscopy. *J. Phys. D: Appl. Phys.*, **42** (14), 142003.
 173. Tan, B., Allen, N., and Rodrigo, H. (2007) Progression of positive corona on cylindrical insulating surfaces. I. Influence of dielectric material. *IEEE Trans. Dielectrics Electr. Insul.*, **14**, 111–118.
 174. Sobota, A., van Veldhuizen, E.M., and Stoffels, W.W. (2008) Discharge ignition near a dielectric. *IEEE Trans. Plasma Sci.*, **36**, 912.
 175. Sobota, A., Lebouvier, A., Kramer, N., Stoffels, W., Manders, F., and Haverlag, M. (2009) Speed of streamers in argon over a flat surface of a dielectric. *J. Phys. D: Appl. Phys.*, **42**, 015211.
 176. Morales, K., Krile, J., Neuber, A., and Krompholz, H. (2007) Dielectric surface flashover at atmospheric conditions with unipolar pulsed voltage excitation. *IEEE Trans. Dielectrics Electr. Insul.*, **14**, 774–782.
 177. Deng, J., Matsuoka, S., Kumada, A., and Hidaka, K. (2010) The influence of residual charge on surface discharge propagation. *J. Phys. D: Appl. Phys.*, **43**, 495203.
 178. Gegot, F., Callegari, T., Aillerie, M., and Boeuf, J. (2008) Experimental protocol and critical assessment of the Pockels method for the measurement of surface charging in a dielectric barrier discharge. *J. Phys. D: Appl. Phys.*, **41**, 135204.
 179. Tanaka, D., Matsuoka, S., Kumada, A., and Hidaka, K. (2009) Two-dimensional potential and charge distributions of positive surface streamer. *J. Phys. D: Appl. Phys.*, **42**, 075204.
 180. Suttikul, T., Sreethawong, T., Sekiguchi, H., and Chavadej, S. (2011) Ethylene epoxidation over alumina- and silica-supported silver catalysts in low-temperature ac dielectric barrier discharge. *Plasma Chem. Plasma Process.*, **31**, 273–290, DOI: 10.1007/s11090-010-9280-1.
 181. Rubin, M. (2001) The history of ozone. The schönbein period, 1839–1868. *Bull. Hist. Chem.*, **26**, 40–56.
 182. Rice, R. and Netzer, A. (1984) *Handbook of Ozone Technologies and Applications, Ozone for Drinking Water Treatment, Vol. II*, Butterworth Publishers, Boston.
 183. Vosmaer, A. (1916) *Ozone: Its Manufacture, Properties and Uses*, Van Nostrand, New York.
 184. Gottschalk, C., Libra, J., and Saupe, A. (2010) *Ozonation of Water and Waste Water: A Practical Guide to Understanding Ozone and its Applications*, Wiley-VCH Verlag GmbH.
 185. Loeb, B. (2010) Editorial. *Ozone: Sci. Eng.*, **32**, 381–382.
 186. Winands, G.J.J., Liu, Z., Pemen, A.J.M., van Heesch, E.J.M., Yan, K., and van Veldhuizen, E.M. (2006) Temporal development and chemical efficiency of positive streamers in a large scale wire-plate reactor as a function of voltage waveform parameters. *J. Phys. D: Appl. Phys.*, **39**, 3010.
 187. Moreau, E. (2007) Airflow control by non-thermal plasma actuators. *J. Phys. D: Appl. Phys.*, **40** (3), 605.
 188. Starikovskii, A., Anikin, N., Kosarev, I., Mintoussov, E., Nudnova, M., Rakitin, A., Roupasov, D., Starikovskaia, S., and Zhukov, V. (2008) Nanosecond-pulsed discharges for plasma-assisted combustion and aerodynamics. *J. Propul. Power*, **24** (6), 1182.

189. Hoder, T., Brandenburg, R., Basner, R., Weltmann, K.D., Kozlov, K., and Wagner, H.E. (2010) A comparative study of three different types of barrier discharges in air at atmospheric pressure by cross-correlation spectroscopy. *J. Phys. D: Appl. Phys.*, **43**, 124009.
190. Kloc, P., Wagner, H.E., Trunec, D., Navrátil, Z., and Fedoseev, G. (2010) An investigation of dielectric barrier discharge in ar and ar/nh3 mixture using cross-correlation spectroscopy. *J. Phys. D: Appl. Phys.*, **43**, 345205.
191. Liu, Z.W., Xu, Y., Yang, X.F., Zhu, A.M., Zhao, G.L., and Wang, W.G. (2008) Determination of the ho2 radical in dielectric barrier discharge plasmas using near-infrared cavity ring-down spectroscopy. *J. Phys. D: Appl. Phys.*, **41**, 045203.
192. Zhao, G., Zhu, A., Wu, J., Liu, Z., and Xu, Y. (2010) Measurement of oh radicals in dielectric barrier discharge plasmas by cavity ring-down spectroscopy. *Plasma Sci. Technol.*, **12**, 166–171.
193. Dong, B., Bauchire, J.M., Pouvesle, J., Magnier, P., and Hong, D. (2008) Experimental study of a dbd surface discharge for the active control of subsonic airflow. *J. Phys. D: Appl. Phys.*, **41**, 155201.
194. Opaits, D., Roupasov, D., Starikovskaia, S., Starikovskii, A., Zavalov, I.N., and Saddoughi, S. (2005) Plasma control of boundary layer using low-temperature non-equilibrium plasma of gas discharge. 43rd AIAA Aerospace Sciences Meeting and Exhibit, Reno, Nevada, paper AIAA 2005-1180.
195. Stoffels, E., Kieft, I., Sladek, R., van den Bedem, L., van der Laan, E., and Steinbuch, M. (2006) Plasma needle for in vivo medical treatment: recent developments and perspectives. *Plasma Sources Sci. Technol.*, **15**, S169–S180.
196. Pokryvailo, A., Wolf, M., Yankelevich, Y., Wald, S., E.M. van Veldhuizen, Grabowski, L., Rutgers, W., Reiser, M., Eckhardt, T., Glocker, B., Kempenaers, P., and Welleman, A. (2006) High-power pulsed corona for treatment of pollutants in heterogeneous media. *IEEE Trans. Plasma Sci.*, **34**, 1731–1743.
197. Grabowski, L., van Veldhuizen, E., Pemen, A., and Rutgers, W. (2007) Breakdown of methylene blue and methyl orange by pulsed corona discharge. *Plasma Sources Sci. Technol.*, **16**, 226–232.
198. Yao, S. (2009) Plasma reactors for diesel particulate matter removal. *Recent Patents Chem. Eng.*, **2**, 67–75.
199. Kalra, C., Gutsol, A., and Fridman, A. (2005) Gliding arc discharges as a source of intermediate plasma for methane partial oxidation. *IEEE Trans. Plasma Sci.*, **33** (1, Part 1), 32–41.
200. Fridman, A., Gutsol, A., Gangoli, S., Ju, Y., and Ombrellol, T. (2008) Characteristics of gliding arc and its application in combustion enhancement. *J. Propul. Power*, **24** (6), 1216–1228.
201. Benstaali, B., Boubert, P., Cheron, B., Addou, A., and Brisset, J. (2002) Density and rotational temperature measurements of the OH degrees and NO degrees radicals produced by a gliding arc in humid air. *Plasma Chem. Plasma Process.*, **22** (4), 553–571.
202. Burlica, R., Kirkpatrick, M., and Locke, B. (2006) Formation of reactive species in gliding arc discharges with liquid water. *J. Electrostat.*, **64** (1), 35–43.
203. Gangoli, S.P., Gutsol, A.F., and Fridman, A.A. (2010) A non-equilibrium plasma source: magnetically stabilized gliding arc discharge: I. Design and diagnostics. *Plasma Sources Sci. Technol.*, **19** (6), 065003.
204. Bruggeman, P. and Leys, C. (2009) Non-thermal plasmas in and in contact with liquids. *J. Phys. D: Appl. Phys.*, **42** (5), 053001.